JPL Publication 89-38

Multiple Symbol Differential Detection of Uncoded and Trellis Coded MPSK

Dariush Divsalar
Marvin K. Simon
Mehrdad Shahshahani

November 15, 1989

National Aeronautics and
Space Administration

Jet Propulsion Laboratory
California Institute of Technology
Pasadena, California

JPL Publication 89-38

Multiple Symbol Differential Detection of Uncoded and Trellis Coded MPSK

Dariush Divsalar
Marvin K. Simon
Mehrdad Shahshahani

November 15, 1989

National Aeronautics and
Space Administration

Jet Propulsion Laboratory
California Institute of Technology
Pasadena, California

The research described in this publication was carried out by the Jet Propulsion Laboratory, California Institute of Technology, under a contract with the National Aeronautics and Space Administration.

Abstract

A differential detection technique for MPSK, which uses a multiple symbol observation interval, is presented and its performance analyzed and simulated. The technique makes use of maximum-likelihood sequence estimation of the transmitted phases rather than symbol-by-symbol detection as in conventional differential detection. As such the performance of this multiple symbol detection scheme fills the gap between conventional (two-symbol observation) differentially coherent detection of MPSK and ideal coherent of MPSK with differential encoding. The amount of improvement gained over conventional differential detection depends on the number of phases, M, and the number of additional symbol intervals added to the observation. What is particularly interesting is that substantial performance improvement can be obtained for only one or two additional symbol intervals of observation. The analysis and simulation results presented are for uncoded and trellis coded MPSK.

Contents

1.0 Introduction 1

2.0 Maximum-Likelihood Detection of MPSK Over an AWGN Channel 2

3.0 Bit Error Probability Performance 6

3.1 Evaluation of the Pairwise Error Probability 7

3.2 Case 1: Conventional DPSK (N=2, M=2) 8

3.3 Case 2: N=3, M=2 9

3.4 General Asymptotic Results 10

4.0 Application to Trellis Coded MDPSK 14

5.0 System Model 15

6.0 Analysis Model 16

7.0 Derivation of Pairwise Error Probability Bound 17

7.1 A Chernoff Bound on Pairwise Error Probability 19

7.2 An Asymptotic (Large SNR) Evaluation of Pairwise Error Probability 22

8.0 Evaluation of an Upper Bound on Bit Error Probability 26

8.1 Evaluation by the Transfer Function Bound Approach 26

8.2 Evaluation Using the Asymptotic Approximation to Pairwise Error Probability 32

8.3 Another Example 32

9.0 Conclusions 33

10.0 References 34

Appendixes

A. Evaluation of the Pairwise Error Probability 51

B. Proof of Eqs. (42) and (48) 53

C. Evaluation of the Chernoff Bound on Pairwise Error Probability 57

D. Asymptotic Evaluation of Certain Integrals of Analytic Functions 60

E. Proof That There Exists a Unique Critical Point of f(z) Along the Imaginary z Axis in the Interval $0 < z < j$ 65

Figures

1. Conventional Differential Detector for MPSK 36

2. Parallel Implementation of Multiple Bit Differential Detector; N=3 37

3. Serial Implementation of Multiple Bit Differential Detector; N=3 38

4. Bit Error Probability Versus E_b/N_0 for Multiple Differential Detection of MPSK; M=2 39

5. Bit Error Probability Versus E_b/N_0 for Multiple Differential Detection of MPSK; M=4 40

6. Bit Error Probability Versus E_b/N_0 for Multiple Differential Detection of MPSK; M=8 41

7. Block Diagram of the Trellis Coded MDPSK System 42

8. QPSK Signal Constellation and Trellis Diagram for Optimum Rate 2/4 Multiple Trellis Coded QPSK 43

9. Trellis With Squared Euclidean Distance Measure That is Mathematically Equivalent to Figure 8 44

10. Trellis Diagram for Conventional Rate 1/2 Trellis Coded QPSK 44

11. Trellis Diagram for Rate 2/4 Multiple Trellis Coded QPSK Equivalent to Figure 10 45

12. Pair-State Transition Diagram for Trellis Diagram of Figure 11 45

13. Analytical and Simulation Results for Bit Error Probability of 2-State, Rate 1/2 Trellis Coded QPSK With Conventional (N=2) and Multiple (N=3) Symbol Differential Detection 46

14. Trellis With Squared Euclidean Distance Measure That is Mathematically Equivalent to Figure 11 47

15. Pair-State Transition Diagram for Trellis Diagram of Figure 14 48

16. Simulation Results for Bit Error Probability of 16 State, Rate 2/3 Trellis Coded 8PSK With Conventional (N=2) and Multiple (N=3) Symbol Differential Detection 49

1.0 Introduction

It is well known that, in applications where simplicity and robustness of implementation take precedence over achieving the best system performance, differential detection is an attractive alternative to coherent detection. Aside from implementation considerations, it is also possible that the transmission environment may be sufficiently degraded, e.g., a multipath fading channel, that acquiring and tracking a coherent demodulation reference signal are difficult if not impossible. Here again, differential detection is a possible, and perhaps the only, solution.

In the past, differential detection of multiple-phase-shift-keying (MPSK) has been accomplished by comparing the received phase in a given symbol interval with that in the previous symbol interval and making a multilevel decision on the difference between these two phases [1]. An implementation of such a receiver and the analysis of its error rate performance on an additive white Gaussian noise (AWGN) channel may also be found in [2: Chap. 5]. In arriving at the results in [1,2], the assumption was made that the received carrier reference phase is constant over at least two symbol intervals and thus has no effect on the decision process when the above-mentioned phase difference is taken. This assumption is crucial to the analysis but is also realistic in many practical applications. Also, since the information is carried in the difference between adjacent received phases, the input information must be differentially encoded before transmission over the channel.

Although differential detection eliminates the need for carrier acquisition and tracking in the receiver, it suffers from a performance penalty (additional required SNR at a given bit error rate) when compared with ideal (perfect carrier phase reference) coherent detection. The amount of this performance penalty increases with the number of phases, M, and is significant for $M \geq 4$. For example, at a bit error probability $P_b = 10^{-5}$, differentially detected BPSK (often abbreviated as DPSK) requires about 0.75 dB more bit energy-to-noise ratio (E_b/N_0) than coherently detected BPSK. For QPSK (M = 4), the difference in E_b/N_0 between differential detection and ideal coherent detection at $P_b = 10^{-5}$ is about 2.2 dB. Finally for 8PSK, the corresponding difference in E_b/N_0 performance between the two is greater than 2.5 dB.

Thus, it is natural to ask: Is there a way of enhancing the conventional

(two symbol observation) differential detection technique so as to recover a portion of the performance lost relative to that of coherent detection, and yet still maintain a simple and robust implementation? Furthemore, if this is possible, what is the tradeoff between the amount of performance recovered and the additional complexity added to the conventional differential detection implementation? The answers to these questions stem from the idea of allowing the observation interval over which symbol decisions are made to be longer than two symbol intervals while at the same time making a *joint* decision on several symbols simultaneously as opposed to symbol-by-symbol detection. As such, one must extend the previous assumption on the duration of time over which the carrier phase is constant to be commensurate with the extended observation interval. For observations on the order of three or four symbol intervals, this is still a reasonable assumption in many applications.

The theoretical framework in which we shall develop this so-called *multiple-bit differential detection* technique is the maximum-likelihood approach to statistical detection. In the next section, we derive the appropriate maximum-likelihood algorithm for differential detection of uncoded MPSK and show how the conventional technique is a special case of this more general model. Since, as mentioned above, we will be making joint symbol decisions in this new configuration, the technique is a form of *maximum-likelihood sequence estimation*, although no coding of the input information is implied. Later on in the report, we extend the theory developed here to the case of trellis-coded MDPSK.

2.0 Maximum-Likelihood Detection of MPSK over an AWGN Channel

Consider the transmission of MPSK signals over an AWGN channel. The transmitted signal in the interval $kT \leq t \leq (k+1)T$ has the complex form

$$s_k = \sqrt{2P}e^{j\phi_k} \tag{1}$$

where P denotes the constant signal power, T denotes the MPSK symbol interval, and ϕ_k the transmitted phase which takes on one of M uniformly distributed values $\beta_m = 2\pi m/M$; m = 0, 1, ..., M-1 around the unit circle. The corresponding received signal is then

$$r_k = s_k e^{j\theta_k} + n_k \tag{2}$$

where n_k is a sample of zero mean complex Gaussian noise with variance

$$\sigma_n^2 = \frac{2N_0}{T} \tag{3}$$

and θ_k is an arbitrary phase introduced by the channel which, in the absence of any side information, is assumed to be uniformly distributed in the interval $(-\pi,\pi)$.

Consider now a received sequence of length N and assume that θ_k is independent of k over the length of this sequence, i.e., $\theta_k = \theta$. Analogous to (2), the received sequence $\underline{r}$ is expressed as

$$\underline{r} = \underline{s}e^{j\theta} + \underline{n} \tag{4}$$

where r_k, s_k, and n_k are, respectively, the k*th* components of the N-length sequences $\underline{r}$, $\underline{s}$, and $\underline{n}$. For the assumed AWGN model, the a posteriori probability of $\underline{r}$ given $\underline{s}$ and θ is

$$p(\underline{r}|\underline{s},\theta) = \frac{1}{\left(2\pi\sigma_n^2\right)^{N/2}} \exp\left\{-\frac{\left\|\underline{r} - \underline{s}e^{j\theta}\right\|^2}{2\sigma_n^2}\right\} \tag{5}$$

where

$$\left\|\underline{r} - \underline{s}e^{j\theta}\right\|^2 = \sum_{i=0}^{N-1} \left|r_{k-i} - s_{k-i}e^{j\theta}\right|^2 \tag{6}$$

Simplifying the right hand side of (6) results in

$$\begin{aligned}\left\|\underline{r} - \underline{s}e^{j\theta}\right\|^2 &= \sum_{i=0}^{N-1}\left[\left|r_{k-i}\right|^2 + \left|s_{k-i}\right|^2\right] - 2\,\mathrm{Re}\left\{\sum_{i=0}^{N-1} r_{k-i}s_{k-i}^*\right\}\cos\theta \\ &\quad - 2\,\mathrm{Im}\left\{\sum_{i=0}^{N-1} r_{k-i}s_{k-i}^*\right\}\sin\theta \\ &= \sum_{i=0}^{N-1}\left[\left|r_{k-i}\right|^2 + \left|s_{k-i}\right|^2\right] - 2\left|\sum_{i=0}^{N-1} r_{k-i}s_{k-i}^*\right|\cos(\theta - \alpha)\end{aligned} \tag{7}$$

where

$$\alpha = \tan^{-1}\frac{\mathrm{Im}\left\{\sum_{i=0}^{N-1} r_{k-i}s_{k-i}^*\right\}}{\mathrm{Re}\left\{\sum_{i=0}^{N-1} r_{k-i}s_{k-i}^*\right\}} \tag{8}$$

Since θ has been assumed to be uniformly distributed, then the a posteriori probabability of $\underline{r}$ given $\underline{s}$ is simply

$$p(\underline{r}|\underline{s}) = \int_{-\pi}^{\pi} p(\underline{r}|\underline{s},\theta)p(\theta)d\theta$$
$$= \frac{1}{\left(2\pi\sigma_n^2\right)^{N/2}} \exp\left\{-\frac{1}{2\sigma_n^2}\sum_{i=0}^{N-1}\left[|r_{k-i}|^2 + |s_{k-i}|^2\right]\right\} I_0\left(\frac{1}{\sigma_n^2}\left|\sum_{i=0}^{N-1} r_{k-i}s_{k-i}^*\right|\right) \tag{9}$$

where $I_0(x)$ is the modified Bessel function of the first kind. Note that for MPSK, $|s_k|^2$ is constant for all phases. Thus, since $I_0(x)$ is a monotonic function of its argument, maximizing $p(\underline{r}\,|\,\underline{s})$ over $\underline{s}$ is equivalent to finding

$$\max_{\underline{s}} \left|\sum_{i=0}^{N-1} r_{k-i}s_{k-i}^*\right|^2 \tag{10}$$

which, using (1), results in the decision rule

$$\text{choose } \underline{\hat{\phi}} \text{ if } \left|\sum_{i=0}^{N-1} r_{k-i}e^{-j\hat{\phi}_{k-i}}\right|^2 \text{ is maximum} \tag{11}$$

where $\underline{\hat{\phi}}$ is a particular sequence of the β_m's. Note that this decision rule has a phase ambiguity associated with it since the addition of an arbitrary fixed phase, say ϕ_a, to all N estimated phases $\hat{\phi}_k, \hat{\phi}_{k-1}, \ldots, \hat{\phi}_{k-N+1}$ results in the same decision for $\underline{\phi}$. Thus, letting $\phi_a = \phi_{k-N+1}$, the above decision rule can be alternately expressed as choosing the sequence $\underline{\hat{\phi}}$ that maximizes the statistic

$$\eta \triangleq \left|\sum_{i=0}^{N-1} r_{k-i}e^{-j(\phi_{k-i}-\phi_{k-N+1})}\right|^2 \tag{12}$$

To resolve the above phase ambiguity, one should differentially encode the phase information at the transmitter. Letting

$$\phi_k = \phi_{k-1} + \Delta\phi_k \tag{13}$$

where now $\Delta\phi_k$ denotes the input data phase corresponding to the k*th* transmission interval and ϕ_k the differentially encoded version of it, then

$$\phi_{k-i} - \phi_{k-N+1} = \sum_{m=0}^{N-i-2} \Delta\phi_{k-i-m} \tag{14}$$

and the above decision statistic becomes

$$\eta = \left| r_{k-N+1} + \sum_{i=0}^{N-2} r_{k-i} e^{-j \sum_{m=0}^{N-i-2} \Delta\phi_{k-i-m}} \right|^2 \tag{15}$$

This statistic implies that we observe the received signal over N symbol time intervals and from this observation make a simultaneous decision on N-1 data phases.

Some special cases of (15) are of interest. For N = 1, i.e., an observation of the received signal over one symbol interval, (15) simplifies to

$$\eta = |r_k|^2 \tag{16}$$

which is completely independent of the input data phases and thus cannot be used for making decisions on differentially encoded MPSK modulation. In fact, the statistic of (16) corresponds to the classical case of noncoherent detection which is not applicable to phase modulation.

Next, let N = 2, in which case (15) becomes

$$\eta = \left| r_{k-1} + r_k e^{-j\Delta\phi_k} \right|^2 = |r_{k-1}|^2 + |r_k|^2 + 2\,\mathrm{Re}\left\{ r_k r_{k-1}^* e^{-j\Delta\phi_k} \right\} \tag{17}$$

This results in the well-known decision rule for conventional MDPSK, namely,

$$\text{choose } \Delta\hat{\phi}_k \text{ if } \mathrm{Re}\left\{ r_k r_{k-1}^* e^{-j\Delta\hat{\phi}_k} \right\} \text{ is maximum} \tag{18}$$

which is implemented in complex form as in Figure 1. Thus, we see from this approach that conventional differential detection of MPSK is the optimum receiver in the sense of minimizing the symbol error probability given that the unknown carrier phase is constant over two symbol times. This result is not new other than, perhaps, the approach taken to demonstrate it.

Now, to see a new structure, we consider (15) for N = 3. Here we have

$$\eta = \left| r_{k-2} + r_k e^{-j(\Delta\phi_k + \Delta\phi_{k-1})} + r_{k-1} e^{-j\Delta\phi_{k-1}} \right|^2 =$$
$$|r_{k-2}|^2 + |r_{k-1}|^2 + |r_k|^2 + 2\,\mathrm{Re}\left\{ r_k r_{k-2}^* e^{-j(\Delta\phi_k + \Delta\phi_{k-1})} \right\}$$
$$+ 2\,\mathrm{Re}\left\{ r_{k-1} r_{k-2}^* e^{-j\Delta\phi_{k-1}} \right\} + 2\,\mathrm{Re}\left\{ r_{k-1} r_{k-1}^* e^{-j\Delta\phi_k} \right\} \qquad (19)$$

Thus, the decision rule becomes

$$\text{choose } \Delta\hat{\phi}_k \text{ and } \Delta\hat{\phi}_{k-1} \text{ if } \mathrm{Re}\left\{ r_k r_{k-1}^* e^{-j\Delta\hat{\phi}_k} + r_{k-1} r_{k-2}^* e^{-j\Delta\hat{\phi}_{k-1}} + r_k r_{k-2}^* e^{-j(\Delta\hat{\phi}_k + \Delta\hat{\phi}_{k-1})} \right\} \text{ is maximum} \qquad (20)$$

Note that the first and second terms of the metric used in the decision rule of (20) are identical to those used to make successive and independent decisions on $\Delta\phi_k$ and $\Delta\phi_{k-1}$, respectively, in conventional MDPSK. The third term in the optimum metric is a combination of the first two and is required to make an optimum *joint* decision on $\Delta\phi_k$ and $\Delta\phi_{k-1}$.

Clearly, a receiver implemented on the basis of (20) will outperform conventional MDPSK. Before demonstrating the amount of this performance improvement as a function of the number of phases, M, we first discuss the implementation of the optimum N = 3 receiver. Figure 2 is a parallel implementation of the decision rule of (20). It should be noted that the M^2 phasors[1] needed to perform the phase rotations of the output $r_k(r_{k-2})^*$ can be obtained using a matrix which performs all possible multiplications of the M phasors $e^{-j\beta 0}$, $e^{-j\beta 1}$, ..., $e^{-j\beta M-1}$ with themselves. Figure 3 is a series implementation of the same decision rule which, although simpler in appearance than Figure 2, requires envelope normalization and additional delay elements.

3.0 Bit Error Probability Performance

To obtain a simple upper bound on the average bit error probability, P_b, of the proposed N-bit detection scheme, we use a union bound analogous to that used for upper bounding the performance of error correction coded systems. In particular, the upper bound on P_b is the sum of the pairwise error probabilities associated with each (N-1)-bit error sequence. Each pairwise error probability is then either evaluated directly or itself upper bounded.

[1] In reality, only M phasors are needed since the sum angle $\Delta\phi_k + \Delta\phi_{k-1}$ when taken modulo 2π ranges over the set $\beta_0, \beta_1, \cdots, \beta_{M-1}$.

Mathematically speaking, let $\underline{\Delta\phi} = (\Delta\phi_k, \Delta\phi_{k-1}, \ldots, \Delta\phi_{k-N+2})$ denote the sequence of N-1 information phases and $\underline{\Delta\hat{\phi}} = (\Delta\hat{\phi}_k, \Delta\hat{\phi}_{k-1}, \ldots, \Delta\hat{\phi}_{k-N+2})$ be the corresponding sequence of detected phases. Let $\underline{u}$ be the sequence of b = (N-1)$\log_2$M information bits that produces $\underline{\Delta\phi}$ at the transmitter and $\underline{u}$ the sequence of b bits that result from the detection of $\underline{\Delta\hat{\phi}}$. Then,

$$P_b \le \frac{1}{b}\frac{1}{M^{N-1}} \sum_{\underline{\Delta\phi}} \sum_{\underline{\Delta\hat{\phi}}} w(\underline{u},\hat{\underline{u}}) \Pr\left\{\hat{\eta} > \eta | \underline{\Delta\phi}\right\} \tag{21}$$

where $w(\underline{u},\hat{\underline{u}})$ denotes the Hamming distance between $\underline{u}$ and $\hat{\underline{u}}$ and $\Pr\left\{\hat{\eta} > \eta | \underline{\Delta\hat{\phi}}\right\}$ denotes the pairwise probability that $\underline{\Delta\hat{\phi}}$ is incorrectly chosen when indeed $\underline{\Delta\phi}$ was sent. The decision statistic η is defined in (15) and the corresponding error statistic $\hat{\eta}$ is identical to (15) with each $\Delta\phi_k$ replaced by $\Delta\hat{\phi}_k$. For symmetric signalling sets (such as MPSK), (21) satisfies a uniform error probability (UEP) criterion, i.e., the probability of error is independent of which input phase sequence $\underline{\Delta\phi}$ is chosen as the correct sequence. Under these conditions, (21) simplifies to

$$P_b \le \frac{1}{(N-1)\log_2 M} \sum_{\underline{\Delta\hat{\phi}} \ne \underline{\Delta\phi}} w(\underline{u},\hat{\underline{u}}) \Pr\left\{\hat{\eta} > \eta | \underline{\Delta\phi}\right\} \tag{22}$$

where $\underline{\Delta\phi}$ is any input sequence (e.g., the null sequence (0,0,...,0) = $\underline{0}$) .

3.1 Evaluation of the Pairwise Error Probability

To compute $\Pr\left\{\hat{\eta} > \eta | \underline{\Delta\phi}\right\}$, we use the approach taken in [3] for evaluating the performance of noncoherent FSK. It is convenient to define

$$w(\underline{\Delta\phi}) = \sum_{i=0}^{N-1} r_{k-i} e^{-j\sum_{m=0}^{N-i-2} \Delta\phi_{k-i-m}} \quad ; \quad w(\underline{\Delta\hat{\phi}}) = \sum_{i=0}^{N-1} r_{k-i} e^{-j\sum_{m=0}^{N-i-2} \Delta\hat{\phi}_{k-i-m}} \tag{23}$$

in which case,

$$\eta = \left|w(\underline{\Delta\phi})\right|^2; \quad \hat{\eta} = \left|w(\underline{\Delta\hat{\phi}})\right|^2 \tag{24}$$

Then, the pairwise error probability $\Pr\{\hat{\eta} > \eta | \underline{\Delta\phi}\}$ is derived in Appendix A as

$$\Pr\{\hat{\eta} > \eta | \underline{\Delta\phi}\} = \frac{1}{2}\left[1 - Q(\sqrt{b}, \sqrt{a}) + Q(\sqrt{a}, \sqrt{b})\right] \tag{25}$$

where $Q(\alpha,\beta)$ is Marcum's Q-function [4] and

$$\begin{Bmatrix} b \\ a \end{Bmatrix} = \frac{E_s}{2N_0}\left[N \pm \sqrt{N^2 - |\delta|^2}\right] \tag{26}$$

with E_S = PT denoting the energy per data symbol and

$$\delta \triangleq \sum_{i=0}^{N-1} e^{\,j \sum_{m=0}^{N-i-2} (\Delta\phi_{k-i-m} - \Delta\hat{\phi}_{k-i-m})} \triangleq \sum_{i=0}^{N-1} e^{\,j \sum_{m=0}^{N-i-2} \delta\phi_{k-i-m}} \tag{27}$$

In (27), it is understood that the summation in the exponent evaluates to zero if the upper index is negative.

Note that for any given N, M, and input data sequence $\underline{\Delta\phi}$, δ can be evaluated for each error sequence $\underline{\Delta\hat{\phi}}$. We now consider the evaluation of (22) and (25) for some special cases.

3.2 Case 1: Conventional DPSK (N = 2, M = 2)

From (27), we immediately get $\delta = 0$ and thus from (26)

$$\begin{Bmatrix} b \\ a \end{Bmatrix} = \begin{Bmatrix} \frac{2E_s}{N_0} \\ 0 \end{Bmatrix} \tag{28}$$

Substituting (28) into (25) gives

$$\Pr\{\hat{\eta} > \eta | \underline{\Delta\phi}\} = \frac{1}{2}\left[1 - Q\left(\sqrt{\frac{2E_s}{N_0}}, 0\right) + Q\left(0, \sqrt{\frac{2E_s}{N_0}}\right)\right] \tag{29}$$

From the definition of the Q-function,

$$Q(\alpha,0) = 1; \quad Q(0,\beta) = \exp\left(-\frac{\beta^2}{2}\right) \tag{30}$$

Since for the binary case the pairwise error probability is indeed equal to the bit error probability, we have from (29) and (30) that

$$P_b = \frac{1}{2}\exp\left(-\frac{E_s}{N_0}\right) \tag{31}$$

which is the well-known result for DPSK.

3.3 Case 2: N = 3, M = 2

Here there are three possible error sequences of length 2. The pertinent results related to the evaluation of (26) and (27) are given below:

$\Delta\phi_k - \Delta\hat{\phi}_k$	$\Delta\phi_{k-1} - \Delta\hat{\phi}_{k-1}$	δ	$\begin{Bmatrix} b \\ a \end{Bmatrix}$
0	π	-1	$\frac{E_s}{N_0}\left[\frac{3}{2} \pm \sqrt{2}\right]$
π	0	$+1$	$\frac{E_s}{N_0}\left[\frac{3}{2} \pm \sqrt{2}\right]$
π	π	$+1$	$\frac{E_s}{N_0}\left[\frac{3}{2} \pm \sqrt{2}\right]$

(32)

Since the Hamming distance $w(\underline{u},\hat{\underline{u}})$ is equal to 1 for the first two error sequences and is equal to 2 for the third sequence, then using (32) in (25) and (26), the upper bound on bit error probability as given by (22) is evaluated as

$$P_b \le 1 - Q\left(\sqrt{\frac{E_b}{N_0}\left(\frac{3}{2}+\sqrt{2}\right)}, \sqrt{\frac{E_b}{N_0}\left(\frac{3}{2}-\sqrt{2}\right)}\right) + Q\left(\sqrt{\frac{E_b}{N_0}\left(\frac{3}{2}-\sqrt{2}\right)}, \sqrt{\frac{E_b}{N_0}\left(\frac{3}{2}+\sqrt{2}\right)}\right) \tag{33}$$

To see how much performance is gained by extending the observation interval for differential detection from N = 2 (conventional) to N = 3, we must compare (33) to (31). Due to the complex form of (33) this comparison is not readily obvious without resorting to numerical evaluation. On the other hand, by examining the asymptotic (large E_S/N_0) behavior of (33) we can get an immediate fix on this gain.

When both arguments of the Q-function are large, the following asymptotic approximations are valid [6]:

$$Q(\alpha,\beta) \cong 1 - \frac{1}{\alpha-\beta}\sqrt{\frac{\beta}{2\pi\alpha}}\exp\left\{-\frac{(\alpha-\beta)^2}{2}\right\}; \quad \alpha >> \beta >> 1$$

$$Q(\alpha,\beta) \cong \frac{1}{\beta-\alpha}\sqrt{\frac{\beta}{2\pi\alpha}}\exp\left\{-\frac{(\beta-\alpha)^2}{2}\right\}; \quad \beta >> \alpha >> 1 \tag{34}$$

Using these approximations, (25) becomes

$$\Pr\left\{\hat{\eta} > \eta | \underline{\Delta\phi}\right\} = \frac{1}{2}\left[\frac{1}{\sqrt{b}-\sqrt{a}}\left(\sqrt{\frac{\sqrt{a/b}}{2\pi}} + \sqrt{\frac{\sqrt{b/a}}{2\pi}}\right)\exp\left\{-\frac{(\sqrt{b}-\sqrt{a})^2}{2}\right\}\right] \tag{35}$$

or, from (26),

$$\begin{aligned}\Pr\left\{\hat{\eta} > \eta | \underline{\Delta\phi}\right\} &= \frac{1}{2\sqrt{2\pi\frac{E_s}{N_0}(N-|\delta|)}}\left(\left(\frac{N-\sqrt{N^2-|\delta|^2}}{N+\sqrt{N^2-|\delta|^2}}\right)^{1/4} + \left(\frac{N+\sqrt{N^2-|\delta|^2}}{N-\sqrt{N^2-|\delta|^2}}\right)^{1/4}\right) \\ &\quad \times \exp\left\{-\frac{E_s}{2N_0}(N-|\delta|)\right\} \\ &= \frac{1}{2\sqrt{\pi\frac{E_s}{N_0}}}\left(\sqrt{\frac{N+|\delta|}{|\delta|(N-|\delta|)}}\right)\exp\left\{-\frac{E_s}{2N_0}(N-|\delta|)\right\}\end{aligned} \tag{36}$$

For N = 3 and M = 2, $|\delta| = 1$ from (32). Thus, (33) becomes

$$P_b \leq \frac{2\sqrt{2}}{\sqrt{\pi\frac{E_s}{N_0}}}\left[\frac{1}{2}\exp\left\{-\frac{E_s}{N_0}\right\}\right] \tag{37}$$

Comparing (37) with (31), we observe that the factor in front of the term in brackets in (37) represents a bound on the improvement in performance obtained by increasing the memory of the decision by one symbol interval from N = 2 to N = 3.

3.4 General Asymptotic Results

In the general case for arbitrary N, the dominant terms in the bit error probability occur for the sequences that result in the minimum value of N -

$|\delta|$. One can easily show that this minimum value will certainly occur for the error sequence $\underline{\Delta\hat{\phi}}$ having N-1 elements equal to the correct sequence $\underline{\Delta\phi}$ and one element with the smallest error. Thus,

$$\begin{aligned}\min_{\underline{\Delta\phi},\underline{\Delta\hat{\phi}}}(N-|\delta|) &= N-\left|N-1+e^{j(\Delta\phi_k-\Delta\hat{\phi}_k)_{\min}}\right| \\ &= N-\sqrt{(N-1)^2+(N-1)(2-d_{\min}^2)+1} \\ &= N-|\delta|_{\max}\end{aligned} \tag{38}$$

where

$$d_{\min}^2 = 4\sin^2\frac{(\Delta\phi_k-\Delta\hat{\phi}_k)_{\min}}{2} = 4\sin^2\frac{\pi}{M} \tag{39}$$

Also note that for $|\delta| = |\delta|_{\max}$, (26) reduces to

$$\begin{Bmatrix} b \\ a \end{Bmatrix} = \frac{E_s}{2N_0}\left[N \pm 2\sqrt{N-1}\sin\frac{\pi}{M}\right] \tag{40}$$

Thus, the average bit error probability is approximately upper bounded by

$$\begin{aligned}P_b \le{}& \frac{1}{(N-1)\log_2 M}\left(\sum_{\underline{\Delta\phi}\neq\underline{\Delta\hat{\phi}}} w(\underline{u},\hat{\underline{u}})\right) \\ &\times \frac{1}{2\sqrt{\frac{E_s}{N_0}}}\left(\sqrt{\frac{N+|\delta|_{\max}}{|\delta|_{\max}\left(N-|\delta|_{\max}\right)}}\right)\exp\left\{-\frac{E_s}{2N_0}\left(N-|\delta|_{\max}\right)\right\}\end{aligned} \tag{41}$$

where $w(\underline{u},\hat{\underline{u}})$ corresponds only to those error sequences that result in $|\delta|_{\max}$.

For the binary case (M = 2), we have from (39) that $d_{\min}^2 = 4$ and hence $N-|\delta|_{\max} = 2$. Similarly, it is straightforward to show (see Appendix B) that the sum of Hamming distances required in (41) is given by

$$\sum_{\underline{\Delta\phi}\neq\underline{\Delta\hat{\phi}}} w(\underline{u},\underline{\hat{u}}) = \begin{cases} 2(N-1); & N>2 \\ 1; & N=2 \end{cases} \tag{42}$$

Thus, (41) simplifies to

$$P_b \leq \frac{2}{\sqrt{\pi \frac{E_s}{N_0}}} \left(\sqrt{\frac{N-1}{N-2}}\right)\left[\frac{1}{2}\exp\left\{-\frac{E_s}{N_0}\right\}\right] \tag{43}$$

which is the generalization of (37) for arbitrary N[2].

Eq. (43) has an interesting interpretation as N gets large. Taking the limit of (43) as $N \to \infty$, we get

$$P_b \leq \frac{1}{\sqrt{\pi \frac{E_s}{N_0}}} \exp\left\{-\frac{E_s}{N_0}\right\} \tag{44}$$

which can be expressed in terms of the asymptotic expansion of the complementary error function,

$$\operatorname{erfc} x \triangleq \frac{2}{\sqrt{\pi}} \int_x^\infty \exp(-y^2)dy \cong \frac{1}{\sqrt{\pi}x} \exp(-x^2) \tag{45}$$

by

$$P_b \leq \operatorname{erfc} \sqrt{\frac{E_s}{N_0}} \tag{46}$$

For *coherent* detection of binary PSK (BPSK) with differential encoding and decoding, the bit error probability performance is given by [2: Chap. 5]

$$P_b = \left(\operatorname{erfc}\sqrt{\frac{E_s}{N_0}}\right)\left(1-\frac{1}{2}\operatorname{erfc}\sqrt{\frac{E_s}{N_0}}\right) \tag{47}$$

which has an asymptotic upper bound identical to (46). Thus, as one might expect, *the performance of multiple symbol differentially detected BPSK approaches that of ideal coherent detection BPSK with differential encoding in the limit as the observation interval (decision memory) approaches infinity.*

---

[2]Note that (43) is not valid for N = 2 since in that case $|\delta|_{max} = 0$ [see (38) and (39)] and thus the inequalities in (34) are not satisfied.

A similar limiting behavior as the above may be observed for other values of M. In particular, it can be shown (see Appendix B) that for M > 2 and a Gray code [2] mapping of bits to symbols, the sum of Hamming distances corresponding to $|\delta|_{max}$ is given by

$$\sum_{\underline{\Delta\phi}\neq\underline{\Delta\hat{\phi}}} w(\underline{u},\underline{\hat{u}}) = \begin{cases} 4(N-1); & N>2 \\ 2; & N=2 \end{cases} \tag{48}$$

Using (48) in (41), we get (for N > 2)

$$P_b \le \frac{2}{(\log_2 M)\sqrt{\pi \frac{E_s}{N_0}}} \left(\sqrt{\frac{N+|\delta|_{max}}{|\delta|_{max}(N-|\delta|_{max})}} \right) \times \exp\left\{ -\frac{E_s}{2N_0}(N-|\delta|_{max}) \right\} \tag{49}$$

where, from (38) and (39),

$$|\delta|_{max} = \sqrt{(N-1)^2 + 2(N-1)(1-2\sin^2\frac{\pi}{M}) + 1} \tag{50}$$

For N = 2, the upper bound on bit error probability becomes

$$P_b \le \frac{1}{(\log_2 M)\sqrt{2\pi \frac{E_s}{N_0}}} \left(\frac{\cos\frac{\pi}{2M}}{\sin\frac{\pi}{2M}\sqrt{\cos\frac{\pi}{M}}} \right) \times \exp\left\{ -\frac{2E_s}{N_0}\sin^2\frac{\pi}{2M} \right\} \tag{51}$$

As N gets large, $|\delta|_{max} \to N - 2\sin^2\frac{\pi}{M}$ and (49) reduces to

$$P_b \le \frac{1}{(\log_2 M)\sqrt{\pi \frac{E_s}{N_0}\sin^2\frac{\pi}{M}}} \exp\left\{ -\frac{E_s}{N_0}\sin^2\frac{\pi}{M} \right\} \equiv \frac{1}{\log_2 M}\operatorname{erfc}\left(\sqrt{\frac{E_s}{N_0}}\sin\frac{\pi}{M} \right) \tag{52}$$

which is identical to the asymptotic bit error probability for *coherent* detection of MPSK with differential encoding and decoding (see [2: Eqs. (5-91), (5-92) and (5-113)])[3].

For example, for QPSK (M=4), the symbol error probability is given by [2: Eq. (5-115)]

$$P_s = 2\,\mathrm{erfc}\left(\sqrt{\frac{E_s}{2N_0}}\right) - 2\,\mathrm{erfc}^2\left(\sqrt{\frac{E_s}{2N_0}}\right) + \mathrm{erfc}^3\left(\sqrt{\frac{E_s}{2N_0}}\right) - \frac{1}{4}\mathrm{erfc}^4\left(\sqrt{\frac{E_s}{2N_0}}\right) \tag{53}$$

Since for a Gray code bit to symbol mapping

$$P_b \cong \frac{P_s}{\log_2 M} = \frac{P_s}{2} \tag{54}$$

then (54) together with (53) has an asymptotic upper bound identical to (52).

Figures 4, 5, and 6 are illustrations of the upper bounds of (49) and (51) for M = 2, 4, and 8, respectively. In each figure, the length (in MPSK symbols) of the observation interval, N, is a parameter varying from N = 2 (conventional MDPSK) to N = ∞ (ideal coherent detection). Also indicated on the figures are computer simulation results corresponding to the exact performance. We observe that, for example, for binary DPSK, extending the observation interval from N = 2 to N = 3 recovers more than half of the E_b/N_0 loss of differential detection versus coherent detection with differential encoding. For M = 4, the improvement in E_b/N_0 performance of N = 3 relative to N = 2 is more than 1 dB which is slightly less than half of the total difference between differential detection and coherent detection with differential encoding.

4.0 Application to Trellis Coded MDPSK

In this part of the report, we extend the idea of multiple differential detection of MPSK to trellis coded modulations (TCM). We will show that a

[3]It should be noted that the result in (52) can be obtained by observing that, for large N, (40) satisfies $\sqrt{b} >> \sqrt{b} - \sqrt{a} > 0$. In this case, (25) can be approximated by [5: Appendix A]

$$\Pr\left\{\hat{\eta} > \eta | \underline{\Delta\phi}\right\} = \frac{1}{2}\left[1 - Q(\sqrt{b},\sqrt{a}) + Q(\sqrt{a},\sqrt{b})\right] \cong \frac{1}{2}\mathrm{erfc}\left(\frac{\sqrt{b}-\sqrt{a}}{\sqrt{2}}\right)$$

Using this relation in (22) gives the asymptotic bit error probability in (52).

combination of a multiple trellis coded modulation (MTCM) [7] with multiplicity equal to N-1 combined with multiple[4] symbol differential detection can potentially yield a significant improvement in performance, even for small N, over that corresponding to conventional trellis coded MDPSK.

The analysis technique that will be employed to obtain upper bounds on the bit error probability performance of the system is equivalent to that used in [8] to assess the performance of conventional trellis coded MDPSK on a fading mobile satellite channel. In fact, it will be shown that the results obtained here have an interesting similarity to those obtained in [8] once an association is made between the squared Euclidean distance measure per trellis branch for conventional differential detection and the equivalent distance measure per trellis branch for multiple symbol differential detection.

5.0 System Model

Figure 7 is a simplified block diagram of the system under investigation. Input bits occurring at a rate R_b are passed through a rate $nk/(n+1)k$ multiple trellis encoder (k is the multiplicity of the code) producing an encoded bit stream at a rate $R_s = [(n+1)k/nk]R_b$. Next, the encoded bits are divided into k groups of n+1 bits each and each group is mapped into a symbol selected from an $M = 2^{n+1}$ - level PSK signal set according to a set partitioning method for multiple trellis codes [7] analogous to that proposed by Ungerboeck [9] for conventional (unit multiplicity) codes. Since the MDPSK symbol rate is R_b/n, it is reasonable, from a conservation of bandwidth standpoint, to compare the performance of this system to an uncoded $M = 2^n$ level DPSK system with the identical input bit rate.

At the receiver, the noise-corrupted signal is differentially detected and the resulting symbols are then inputted to the trellis decoder which is implemented as a Viterbi algorithm. In selecting a decoding metric, a tradeoff exists between simplicity of implementation and the optimality associated with the degree to which the metric matches the differential detector output statistics.

---

[4]One must be careful not to confuse the multiplicity of the trellis code with the multiplicity of the differential detection scheme although, as we shall soon see, the two are indeed related.

For the case of uncoded MDPSK, a metric based on minimizing the distance between the received and transmitted signal vectors is optimum in the sense of a minimum probability of error test. The specific forms of this metric for conventional and multiple differential detection were described in Section 2.0. For conventional trellis-coded MDPSK, the metric takes on the form of a minimum squared Euclidean distance metric. For multiple symbol detection of MTCM, the form of the metric is quite different. Nevertheless, as we shall soon see, by a suitable modification of the multiple trellis code design, the appropriate metric can be converted once again into a minimum squared Euclidean distance metric. The so-called "equivalent" multiple trellis code that results from this modification then becomes the key tool used for analyzing the performance of the system.

6.0 Analysis Model

We denote a coded symbol sequence of length N_S by

$$\underline{x} = (x_1, x_2, \cdots, x_{N_s}) \tag{55}$$

where the k*th* element of $\underline{x}$, namely, x_k, represents the transmitted MPSK symbol in the k*th* transmission interval and, in general, is a nonlinear function of the state of the encoder and the nk information bits at its input. Before transmission over the channel, the sequence $\underline{x}$ is differentially encoded producing the sequence $\underline{s}$. In phasor notation, s_k and s_{k+1} can be written as

$$\begin{aligned} s_k &= \sqrt{2P}e^{j\phi_k} \\ s_{k+1} &= s_k x_{k+1} = \sqrt{2P}e^{j(\phi_k + \Delta\phi_{k+1})} = \sqrt{2P}e^{j\phi_{k+1}} \end{aligned} \tag{56}$$

where $E_S = rE_b$ is the energy per MDPSK symbol and

$$x_k = e^{j\Delta\phi_k} \tag{57}$$

is the phasor representation of the MPSK symbol $\Delta\phi_k$ assigned by the mapper in the k*th* transmission interval.

The corresponding received signal in the k*th* transmission interval is given by (2) with s_k now defined as in (56) and the noise sample, n_k, defined as before with variance given by (3).

Consider now a received sequence of length N_S and assume that θ_k is independent of k over the length of this sequence, i.e., $\theta_k = \theta$. Then, the received sequence $\underline{r}$ is expressed as in (4) where r_k, s_k, and n_k are, respectively, the *kth* components of the N_S-length sequences $\underline{r}$, $\underline{s}$, and $\underline{n}$. Since the detection scheme will be independent of θ, we can furthermore set $\theta = 0$ without any loss of generality.

To apply the notion of multiple symbol differential detection to trellis coded MPSK, the decision statistic of (15) must be associated with a *branch* in the trellis diagram. To do this, we construct a multiple trellis code of multiplicity k = N-1. (The procedure for designing this code will be discussed later on in the publication.) Thus, we can envision the transmitted sequence, $\underline{x}$, of (55) as being partitioned into $B = N_S/k = N_S/(N-1)$ subsequences[5], i.e.,

$$\underline{x} = (\underline{x}^{(1)}, \underline{x}^{(2)}, \ldots, \underline{x}^{(B)}) \tag{58}$$

with each subsequence $\underline{x}^{(i)} = (x_{i1}, x_{i2}, \ldots, x_{ik})$ representing an assignment to a trellis branch. Similarly, a received sequence, $\underline{r}$, of length N_S is associated with a path of length B branches in the trellis diagram. Once this association is made, computation of bit error probability for the system follows along the lines of the approach taken in [7]. The details of the analysis are presented in the following sections.

7.0 Derivation of Pairwise Error Probability Bound

To find an upper bound on the average bit error probability performance of the system, we must first find the pairwise error probability which represents the probability of choosing the coded sequence $\hat{\underline{x}} = (\hat{x}_1, \hat{x}_2, \ldots, \hat{x}_{N_s}) = (\hat{\underline{x}}^{(1)}, \hat{\underline{x}}^{(2)}, \ldots, \hat{\underline{x}}^{(B)})$ instead of $\underline{x} = (x_1, x_2, \ldots, x_{N_s}) = (\underline{x}^{(1)}, \underline{x}^{(2)}, \ldots, \underline{x}^{(B)})$. Letting η_i denote the maximum-likelihood metric for the correct data phase sequence on the *ith* trellis branch and computed in accordance with (15), then the pairwise error probability is given by

$$P(\underline{x} \to \hat{\underline{x}}) = \Pr\left\{ \sum_{i=1}^{B} \hat{\eta}_i > \sum_{i=1}^{B} \eta_i \middle| \underline{\Delta\phi} \right\} \tag{59}$$

[5]Since N_S is arbitrary, we can choose it such that $N_S/(N-1)$ is integer.

Here $\hat{\eta}_i$ denotes the metric computed for the data phase sequence associated with the *ith* trellis branch of the incorrect path, $\underline{\Delta\phi}$ denotes the transmitted data phase sequence for the correct path, and B is the length (in branches) of the correct and incorrect paths. Also, since the channel is additive white Gaussian noise (AWGN), the summations in (59) represent sums of independent random variables.

An exact evaluation of (59) in closed form is difficult if not impossible. At first glance it might appear that the decision variable in (59) is a special case of the quadratic form given in [10: Eq. (4B.1)] and thus the pairwise error probability would be given by [10: Eq. (4B.21)]. Unfortunately, however, the development in [10: Appendix 4B] requires that the second central moments of the complex-valued random variables η_i, $\hat{\eta}_i$; i = 1,2,...,B be *independent of i*. While indeed the variances of these random variables are independent of i, the covariance of η_i and $\hat{\eta}_i$ is directly proportional to δ_i (see Eq. (A-5)) defined by

$$\delta_i \stackrel{\Delta}{=} \sum_{n=0}^{N-1} e^{\,j \sum_{m=0}^{N-n-2} \left(\Delta\phi^{(i)}_{k-n-m} - \Delta\hat{\phi}^{(i)}_{k-n-m}\right)} \stackrel{\Delta}{=} \sum_{n=0}^{N-1} e^{\,j \sum_{m=0}^{N-n-2} \delta\phi^{(i)}_{k-n-m}} \qquad (60)$$

and thus depends on i. In (60), the data phases that appear in the exponent are the elements of $\underline{\Delta\phi^{(i)}}$ and $\underline{\Delta\hat{\phi}^{(i)}}$ which denote the *ith* subsequences of $\underline{\Delta\phi}$ and $\underline{\Delta\hat{\phi}}$, respectively.

In principle, then, there are two approaches one can take to evaluating (59). The first is to derive a Chernoff bound [11] on (59) using a method similar to that taken in [8]. This method has the advantage (as we shall soon see) of enabling the upper bound on bit error probability to be obtained using the transfer function bound approach applied to trellis coded modulations in [7]. It has the disadvantage (typical of Chernoff bounds) of resulting in a loose upper bound on bit error probability.

The second approach is to try to directly approximate (rather than upper bound) the result in (59) for large signal-to-noise ratio (SNR). In Section 3.0 we saw for the uncoded that, despite the fact that we were able to exactly evaluate the pairwise error probability (equivalent to evaluating (59) for a path consisting of a single trellis branch, i.e., B = 1), we eventually approximated that result for large SNR and showed that the results agreed extremely well with those obtained from simulation. Also, the asymptotic (large SNR) form of the bit error probability expression had the advantage of allowing direct comparison with an

analogous expression for conventional (no multiple symbol observation) MDPSK. The disadvantage of this approach is that the expression for the approximate pairwise error probability that results cannot be put in a form that allows evaluation of the upper bound on bit error probability by the transfer function bound approach. Thus, in this part of the report, we shall consider both approaches because of their respective merits.

7.1 A Chernoff Bound on Pairwise Error Probability

A Chernoff upper bound [6] on the pairwise error probability of (59) is evaluated in Appendix C with the result

$$P(\underline{x} \to \underline{\hat{x}}) \le \prod_{\substack{i=1 \\ \Delta\underline{\hat{\phi}}^{(i)} \neq \Delta\underline{\phi}^{(i)}}}^{B} \frac{\exp\left\{-\frac{E_s}{N_0}\frac{\lambda(1-\lambda N)\left[N^2-|\delta_i|^2\right]}{1-\lambda^2\left[N^2-|\delta_i|^2\right]}\right\}}{1-\lambda^2\left[N^2-|\delta_i|^2\right]} \tag{61}$$

where δ_i is given by (60).

The expression in (61) bears a striking resemblance to that which characterizes the pairwise error probability of conventional differential detection of trellis coded MDPSK. In particular, letting $\rho_n = 1$ (no fading) and $\lambda = 2\lambda_0$ in [8: Eq. (25)], we get

$$P(\underline{x} \to \underline{\hat{x}}) \le \prod_{\substack{i=1 \\ \hat{x}_i \neq x_i}}^{B} \frac{\exp\left\{-\frac{E_s}{N_0}\frac{\lambda(1-2\lambda)|\hat{x}_i - x_i|^2}{1-\lambda^2|\hat{x}_i - x_i|^2}\right\}}{1-\lambda^2|\hat{x}_i - x_i|^2} \tag{62}$$

Note that for N = 2 (conventional differential detection) and M = 2 (binary DPSK),

$$|\hat{x}_i - x_i|^2 = 4$$
$$\delta_i = 0 \tag{63}$$

in which case, (61) agrees with (62).

Comparing (61) with (62) we observe that, for multiple symbol differential detection, the equivalent squared Euclidean distance measure *per trellis branch*

is $N^2 - |\delta|^2$. We now examine in detail the algebraic structure of $N^2 - |\delta|^2$. In particular, we shall show how $N^2 - |\delta|^2$ can be expressed as a *squared Euclidean distance* of an "equivalent" trellis code with larger multiplicity. Once this association is made, this "equivalent" trellis code then serves as the mathematical tool by which the foregoing analysis in [3] can be directly applied here.

7.1.1 The Construction of an Equivalent Multiple Trellis Code with Squared Euclidean Distance Measure

Here we show how to take a trellis code of multiplicity N-1 and distance measure $N^2 - |\delta|^2$ and construct an equivalent (in performance) code with larger multiplicity but a *squared Euclidean distance measure.* For simplicity of explanation, we will start with the case N = 3 which corresponds to only one additional symbol of observation relative to conventional differential detection.

From (57) and (60), we have that

$$N^2 - |\delta_i|^2 = N^2 - \left| \sum_{n=0}^{N-1} \prod_{m=0}^{N-n-2} x_{k-n-m}^{(i)} \hat{x}_{k-n-m}^{(i)*} \right|^2$$

$$= N^2 - \left| 1 + \sum_{n=0}^{N-2} \prod_{m=0}^{N-n-2} x_{k-n-m}^{(i)} \hat{x}_{k-n-m}^{(i)*} \right|^2 \qquad (64)$$

For N = 2, (64) simplifies to

$$N^2 - |\delta_i|^2 = 4 - \left| 1 + x_k^{(i)} \hat{x}_k^{(i)*} \right|^2 \qquad (65)$$

Since there is only one MPSK symbol per trellis branch, i.e., multiplicity equal to one, we can simplify the notation in (65) to

$$N^2 - |\delta_i|^2 = 4 - \left| 1 + x_i \hat{x}_i^* \right|^2 = 4 - \left(1 + |x_i|^2 |\hat{x}_i|^2 + 2\,\mathrm{Re}\{x_i \hat{x}_i^*\} \right)$$

$$= 2 - 2\,\mathrm{Re}\{x_i \hat{x}_i^*\} = |x_i - \hat{x}_i|^2 \qquad (66)$$

Thus, for conventional differential detection, $N^2 - |\delta|^2$ yields the squared Euclidean distance measure as one would expect.

For N = 3, (64) becomes

$$
\begin{aligned}
N^2 - |\delta_i|^2 &= 9 - \left|1 + x_k^{(i)}\hat{x}_k^{(i)*}x_{k-1}^{(i)}\hat{x}_{k-1}^{(i)*} + x_{k-1}^{(i)}\hat{x}_{k-1}^{(i)*}\right|^2 \\
&= 9 - \left(3 + 2\,\mathrm{Re}\left\{x_k^{(i)}\hat{x}_k^{(i)*}x_{k-1}^{(i)}\hat{x}_{k-1}^{(i)*}\right\} + 2\,\mathrm{Re}\left\{x_{k-1}^{(i)}\hat{x}_{k-1}^{(i)*}\right\} + 2\,\mathrm{Re}\left\{x_k^{(i)}\hat{x}_k^{(i)*}\right\}\right) \\
&= 6 - \left(2 - \left|x_k^{(i)}x_{k-1}^{(i)} - \hat{x}_k^{(i)}\hat{x}_{k-1}^{(i)}\right|^2\right) - \left(2 - \left|x_{k-1}^{(i)} - \hat{x}_{k-1}^{(i)}\right|^2\right) - \left(2 - \left|x_k^{(i)} - \hat{x}_k^{(i)}\right|^2\right) \\
&= \left|x_{k-1}^{(i)} - \hat{x}_{k-1}^{(i)}\right|^2 + \left|x_k^{(i)} - \hat{x}_k^{(i)}\right|^2 + \left|x_k^{(i)}x_{k-1}^{(i)} - \hat{x}_k^{(i)}\hat{x}_{k-1}^{(i)}\right|^2
\end{aligned}
\tag{67}
$$

The first two terms in (67) represent the squared Euclidean distances associated with the two symbols assigned to the i*th* trellis branch and as such their sum would be the squared Euclidean distance for this branch. The third term in (67) can be interpreted as follows. Note that the product of two MPSK symbols, say x_k and x_m, is indeed another MPSK symbol whose phase is the modulo M sum of the phases of x_k and x_m. Thus, if the MPSK symbols are represented by their equivalent M-ary numbers, e.g., $e^{j2\pi m/M} \rightarrow m$, then the third term in (17) represents the squared Euclidean distance associated with a symbol which is *the modulo M sum of the first two symbols assigned to that trellis branch.*

As a simple example of the above construction, consider the multiple trellis code illustrated in Figure 8 which has multiplicity k = N - 1 = 2. This code is the optimum 2 state, k = 2, rate 2/4 trellis coded QPSK designed for the AWGN. Computing the performance of this code with a three symbol multiple differential detection scheme, the distance measure $N^2 - |\delta|^2$ is then, according to the above, mathematically the same as computing the performance of the k = 3 trellis code in Figure 9 and a squared Euclidean distance measure. Note that the third symbol assigned to each branch in Figure 9 is the modulo 4 sum of the first two symbols on each path of that branch.

The above technique for generating the equivalent code can be generalized to arbitrary N. In particular, from (64) it is straightforward to show that[6]

[6]For simplicity of notation, we omit the "i's" on the variables with the understanding that we are dealing with the i*th* branch.

$$N^2-|\delta|^2=\sum_{n_1=0}^{N-2}\left|x_{k-n_1}-\hat{x}_{k-n_1}\right|^2+\sum_{n_1=0}^{N-3}\sum_{n_2=1}^{N-2}\left|x_{k-n_1}x_{k-n_2}-\hat{x}_{k-n_1}\hat{x}_{k-n_2}\right|^2$$
$$+\sum_{n_1=0}^{N-4}\sum_{n_2=1}^{N-3}\sum_{n_3=2}^{N-2}\left|x_{k-n_1}x_{k-n_2}x_{k-n_3}-\hat{x}_{k-n_1}\hat{x}_{k-n_2}\hat{x}_{k-n_3}\right|^2$$
$$+\cdots\left|x_kx_{k-1}\cdots x_{k-N+2}-\hat{x}_k\hat{x}_{k-1}\cdots\hat{x}_{k-N+2}\right|^2 \qquad (68)$$

Once again the first term in (68) represents the squared Euclidean distance associated with a branch in the N-1 multiplicity trellis code whereas the remaining terms represent the squared Euclidean distances of the additional symbols that must be assigned to each branch in accordance with modulo M sums of the previous symbols.

It is important to emphasize that the trellis code of Figure 9 (or, more generally, the one that would be constructed from (68)) is strictly a mathematical tool that is useful for performance analysis. The actual trellis code that would be used for an N = 3 multiple differential detection of rate 2/4 trellis coded QPSK would be a multiplicity 2 code such as that illustrated in Figure 8.

7.2 An Asymptotic (Large SNR) Evaluation of Pairwise Error Probability

As previously mentioned, finding an exact closed form expression for the pairwise probability of (59) is difficult due to the dependence of the covariance of η_i and $\hat{\eta}_i$ on the summation index i. Nevertheless, if one is willing to settle for asymptotic (large E_S/N_0) results, then it is possible to define a procedure which will allow approximate evaluation of pairwise error probability.

To see how this comes about we first recognize that the decision variable is a special case of the quadratic form discussed in [10: Appendix 4B]. Thus, following the approach taken there, it is straightforward to show that for the specific case at hand here where the second central moments depend on i, [10: Eq. (4B.9)] generalizes to

$$P(\underline{x}\to\underline{\hat{x}})=-\frac{\prod_{i=1}^{B}v_i^2}{2\pi j}\int_{-\infty+j\varepsilon}^{\infty+j\varepsilon}\frac{1}{v}\prod_{i=1}^{B}\frac{\exp\left\{\dfrac{v_i^2\left[jv\alpha_{2i}-v^2\alpha_{1i}\right]}{v^2+v_i^2}\right\}}{v^2+v_i^2}dv \qquad (69)$$

where

$$\alpha_{1i} = (2P)\left(\frac{2NN_0}{T}\right)\left[N^2 - |\delta_i|^2\right]$$

$$\alpha_{2i} = (2P)\left[N^2 - |\delta_i|^2\right]$$

$$v_i = \left[\left(\frac{2N_0}{T}\right)\sqrt{N^2 - |\delta_i|^2}\right]^{-1} \tag{70}$$

with δ_i defined in (60) and $\varepsilon > 0$ a parameter that can be selected, as we shall soon see, for convenience in defining the contour path of integration. At this point, we cannot proceed further with the procedure taken in [10: Appendix 4B] due to the dependence of v_i on i.

A technique for evaluating (70) in the limit of large $PT/N_0 = E_S/N_0$ is discussed in Appendix D and is based on a variation of the method of stationary phase for analytic functions [13]. In order to apply this technique to (70), we first rewrite it in the normalized form

$$P(\underline{x} \to \hat{\underline{x}}) = -\frac{1}{2\pi j}\int_{-\infty+j\varepsilon'}^{\infty+j\varepsilon'} \frac{1}{z}\prod_{i=1}^{B}\frac{1}{\xi_i^2 z^2 + 1}\exp\left\{\frac{E_s}{N_0}\sum_{i=1}^{B}\frac{j\xi_i z\beta_{2i} - \xi_i^2 z^2\beta_1}{\xi_i^2 z^2 + 1}\right\}dz \tag{71}$$

where

$$\beta_1 = N$$

$$\beta_{2i} = \sqrt{N^2 - |\delta_i|^2}$$

$$\xi_i = \frac{v_{i_{\min}}}{v_i} = \sqrt{\frac{N^2 - |\delta_i|^2}{N^2 - |\delta_{i_{\min}}|^2}} \le 1 \tag{72}$$

and $\varepsilon' = \varepsilon / v_{i_{\min}}$ where $i_{\min}$ is the value of i that results in the minimum value of $|\delta_i|$, i.e., the trellis branch along the error event path with the largest equivalent squared Euclidean distance $N^2 - |\delta_i|^2$. The integral in (71) is now in the form of (D-1) where

$$g(z) = \frac{1}{z}\prod_{i=1}^{B}\frac{1}{\xi_i^2 z^2 + 1}$$

$$f(z) = \sum_{i=1}^{B}\frac{\xi_i z\beta_{2i} + j\xi_i^2 z^2\beta_1}{\xi_i^2 z^2 + 1} \tag{73}$$

Before considering the general result for an error event path with an

arbitrary number of branches B, we shall show that, for B = 1 (a one branch path), this approach gives the identical result to (36) for the uncoded case. In particular, for B = 1, we have from (72) that $\xi_1 = 1$, and thus letting $\delta = \delta_1$, the appropriate[7] critical point (value of z where f'(z) = 0) of (73) is given by

$$z_0 = j\sqrt{\frac{N-|\delta|}{N+|\delta|}} < j \tag{74}$$

Also, note that since the integration contour in (71) is selected to pass through the critical point of (74), then

$$\varepsilon' = \sqrt{\frac{N-|\delta|}{N+|\delta|}} \tag{75}$$

The real and imaginary parts of f(z) evaluated at the critical point of (74) are given by

$$\begin{aligned} \phi_1(z_0) &= \mathrm{Re}\{f(z_0)\} = 0 \\ \phi_2(z_0) &= \mathrm{Im}\{f(z_0)\} = \frac{N-|\delta|}{2} \end{aligned} \tag{76}$$

Also,

$$\begin{aligned} f''(z_0) &= \frac{j}{2}\frac{(N+|\delta|)^2}{|\delta|} \\ g(z_0) &= -j\sqrt{\frac{N+|\delta|}{N-|\delta|}}\frac{N+|\delta|}{2|\delta|} \end{aligned} \tag{77}$$

Finally, substituting (76) and (77) into (D-13) gives the desired result

$$P(\underline{x} \to \underline{\hat{x}}) = \Pr\{\hat{\eta} > \eta | \underline{\Delta\phi}\} \cong \frac{1}{2\sqrt{\pi \frac{E_s}{N_0}}}\left(\sqrt{\frac{N+|\delta|}{|\delta|(N-|\delta|)}}\right)\exp\left\{-\frac{E_s}{2N_0}(N-|\delta|)\right\} \tag{78}$$

which agrees with (36).

[7]Another critical point of f(z) occurs at

$$z_0 = j\sqrt{\frac{N+|\delta|}{N-|\delta|}} > j$$

However, this point results in the integration contour passing through one of the singularites of g(z) at z = j and thus, in accordance with Appendix D, is not allowable.

For an error event with an arbitrary number of branches, B, we reason as follows. Since the parameters $\{\xi_i;\ i = 1,2,...,B\}$ in (72) have been defined such that their values are all less than or equal to unity, then from (73) we observe that, aside from the singularity of g(z) at z = 0, all of the singularities of f(z) and g(z) lie on the imaginary z axis in the interval $j \le z \le \infty$. Furthermore, it is shown in Appendix E that there exists a unique critical point of f(z) in the interval $0 \le z \le j$. Denoting this critical point by $z_0 = jy_0$ (unfortunately, one cannot, in general, find a closed form expression for z_0 analogous to (74) and thus one must resort to numerical evaluation), then the integration contour in (71) should again be selected to pass through this point, i.e., choose $\varepsilon' = y_0$. Furthermore, the contour should be tailored so that it does not pass through any of the other critical points of f(z) should they occur at values of $z = a + j\varepsilon'$; $a \neq 0$.

From (73), we observe that for $z_0 = jy_0$, $f(z_0)$ and $g(z_0)$ are purely imaginary, i.e.,

$$f(jy_0) = j\sum_{i=1}^{B} \frac{\beta_{2i}\xi_i y_0 - \beta_{1i}\xi_i^2 y_0^2}{1-\xi_i^2 y_0^2} \stackrel{\Delta}{=} j\phi_1(y_0)$$

$$g(jy_0) = -j\left[\frac{1}{y_0}\prod_{i=1}^{B}\frac{1}{1-\xi_i^2 y_0^2}\right] \stackrel{\Delta}{=} -j\phi_2(y_0) \tag{79}$$

Also, the second derivative of f(z) evaluated at $z = z_0$ is also purely imaginary and given by

$$f''(jy_0) = j\sum_{i=1}^{B} 2\xi_i^2\left[\frac{\beta_1 - 3\beta_{2i}\xi_i y_0 + 3\beta_{1i}\xi_i^2 y_0^2 - \beta_{2i}\xi_i^3 y_0^3}{\left(1-\xi_i^2 y_0^2\right)^3}\right] \stackrel{\Delta}{=} j\phi_3(y_0) \tag{80}$$

Then, using the results of Appendix D, in particular, Eq. (D-13), the pair-wise error probability of (71) is asymptotically approximated by

$$P(\underline{x} \to \hat{\underline{x}}) \cong \frac{1}{\sqrt{2\pi\dfrac{E_s}{N_0}}}\left(\frac{\phi_2(y_0)}{\sqrt{\phi_3(y_0)}}\right)\exp\left\{-\frac{E_s}{N_0}\phi_1(y_0)\right\} \tag{81}$$

which is of the same functional form as (78).

8.0 Evaluation of an Upper Bound on Bit Error Probability

An upper union bound on the average bit error probability is obtained from the pairwise error probability as

$$P_b \le \sum_{\underline{x},\underline{\hat{x}} \in C} \sum a(\underline{x},\underline{\hat{x}}) p(\underline{x}) P(\underline{x} \to \underline{\hat{x}}) \tag{82a}$$

where $a(\underline{x},\underline{\hat{x}})$) is the number of bit errors that occur when $\underline{x}$ is transmitted and $\underline{x}$ is chosen by the decoder, p($\underline{x}$) is the a priori probability of transmitting $\underline{x}$ and C is the set of all coded sequences. If the pairwise error probability is upper Chernoff bounded as in Section 7.1, then one must in addition optimize over the Chernoff parameter, in which case (82a) becomes

$$P_b \le \min_{\lambda} \sum_{\underline{x},\underline{\hat{x}} \in C} \sum a(\underline{x},\underline{\hat{x}}) p(\underline{x}) P(\underline{x} \to \underline{\hat{x}}) \tag{82b}$$

8.1 Evaluation by the Transfer Function Bound Approach

When the pairwise error probability is upper Chernoff bounded, then an efficient procedure for evaluating (82b) is the transfer function found approach applied to multiple trellis coded modulations in [7]. In particular, the trellis codes are represented by a pair-state transition diagram [14]. Each pair-state $(s_i,\hat{s}_i)$ corresponds to a pair of states s_i and $\hat{s}_i$ in the trellis diagram. Thus, a transition between pair-states $(s_i,\hat{s}_i)$ and $(s_{i+1},\hat{s}_{i+1})$ in the transition diagram corresponds to a pair of transitions in the trellis diagram, i.e., s_i to s_{i+1} and $\hat{s}_i$ to $\hat{s}_{i+1}$. Associated with each of these trellis diagram transitions are the k' MPSK symbols[8] corresponding to a sequence of nk input bits (an information symbol) to the multiple trellis encoder. Thus, the transition between two pair-states in the transition diagram is characterized by a function of the squared Euclidean distance $|\hat{z}_i - z_i|^2$; i = 1,2,...,k' between the corresponding k' MPSK output symbols[9] and the Hamming distance Ω between the corresponding input bit sequences.

---

[8]Here, k' refers to the extended multiplicity of the equivalent code as discussed in the previous section.

[9]Here z_i and $\hat{z}_i$ denote the correct and incorrect MPSK symbols assigned to a trellis branch in the equivalent code with extended multiplicity. As such, the first k of these symbols will be identical to the x_i's and $\hat{x}_i$'s, respectively, whereas the remaining symbols represent modulo M sums of these first k in accordance with the construction procedure discussed in Section 8.1.

Based on the above discussion, each branch between pair states in the transition diagram has a gain G of the form

$$G=\sum\frac{1}{2^{nk}}I^{\Omega}\frac{\exp\left\{-\frac{E_s}{N_0}\frac{\lambda(1-\lambda N)\sum_{i=1}^{k'}\left|\hat{z}_i-z_i\right|^2}{1-\lambda^2\sum_{i=1}^{k'}\left|\hat{z}_i-z_i\right|^2}\right\}}{1-\lambda^2\sum_{i=1}^{k'}\left|\hat{z}_i-z_i\right|^2}=\sum\frac{1}{2^{nk}}I^{\Omega}f\left(\sum_{i=1}^{k'}\left|\hat{z}_i-z_i\right|^2,\lambda\right) \quad (83)$$

where I is an index, nk is the number of bits input to the trellis encoder in each transmission interval, and

$$f(x,\lambda)\overset{\Delta}{=}\frac{D^{\frac{4\lambda(1-\lambda N)x}{1-\lambda^2 x}}}{1-\lambda^2 x} \quad (84)$$

with D the Bhattacharyya parameter [11,14] defined by

$$D\overset{\Delta}{=}\exp\left(-\frac{E_s}{4N_0}\right) \quad (85)$$

Also in (83), the summation accounts for the possibility of parallel paths between states in the trellis diagram. The transfer function (the sum of all possible path gains) of the transition diagram is denoted by T(D,I) and, by comparison with (82b), the upper bound on average bit error probability is given by

$$P_b\le\min_{\lambda}\frac{1}{nk}\frac{d}{dI}T(D,I)\Big|_{I=1} \quad (86)$$

8.1.1 A Simple Example

To illustrate the foregoing theory, we consider, as a baseline, the simple case of a 2 state, rate 1/2 trellis coded QPSK designed for the AWGN. The appropriate trellis diagram for such an Ungerboeck design is illustrated in Figure 10. If indeed we are to detect this coded modulation differentially with N symbol observation, then we must *first* construct a multiple trellis code with multiplicity k = N-1 which would have identical performance as the original k = 1 code of Figure 10 if conventional differential detection (N = 2) were used for both.[10]

[10]Note that the construction of such an equivalent (same performance) multiple trellis code from a unit multiplicity (Ungerboeck-type) trellis code can always be performed whereas the reverse is not necessarily true. Also note that the multiple trellis code does not require a different encoder than that used for the unit multiplicity code.

The particular case we shall consider here is N = 3. Thus, we need to transform the trellis diagram of Figure 4 into an equivalent multiple trellis diagram with multiplicity k = 2. The procedure for doing this is to perform a particular type of Cartesian product of the transition matrix of the code in Figure 10 with itself. Letting

$$\mathbf{T}=\begin{bmatrix} x_{00} & x_{01} \\ x_{10} & x_{11} \end{bmatrix} \tag{87}$$

represent the transition matrix of a 2 state code with no parallel paths, i.e., x_{ij} is the MPSK symbol assigned to the branch corresponding to the transition from state "i" to state "j", then the appropriate transition matrix for the equivalent multiple trellis code is

$$\mathbf{T}^{(2)} \triangleq \begin{bmatrix} x_{00} & x_{01} \\ x_{10} & x_{11} \end{bmatrix} \otimes \begin{bmatrix} x_{00} & x_{01} \\ x_{10} & x_{11} \end{bmatrix} \triangleq \begin{bmatrix} \begin{pmatrix} x_{00},x_{00} \\ x_{01},x_{10} \end{pmatrix} & \begin{pmatrix} x_{00},x_{01} \\ x_{01},x_{11} \end{pmatrix} \\ \begin{pmatrix} x_{10},x_{00} \\ x_{11},x_{10} \end{pmatrix} & \begin{pmatrix} x_{10},x_{01} \\ x_{11},x_{11} \end{pmatrix} \end{bmatrix} \tag{88}$$

From (75), we see that each branch in the equivalent trellis code is characterized by two parallel paths with code symbol assignments in accordance with the 2-tuples in $\mathbf{T}^{(2)}$.

Applying (87) to Figure 10, we get

$$\mathbf{T}=\begin{bmatrix} 0 & 2 \\ 1 & 3 \end{bmatrix} \tag{89}$$

and thus, from (75), the transition matrix of the equivalent code is given by

$$\mathbf{T}^{(2)} \triangleq \begin{bmatrix} 0 & 2 \\ 1 & 3 \end{bmatrix} \otimes \begin{bmatrix} 0 & 2 \\ 1 & 3 \end{bmatrix} \triangleq \begin{bmatrix} \begin{pmatrix} 0,0 \\ 2,1 \end{pmatrix} & \begin{pmatrix} 0,2 \\ 2,3 \end{pmatrix} \\ \begin{pmatrix} 1,0 \\ 3,1 \end{pmatrix} & \begin{pmatrix} 1,2 \\ 3,3 \end{pmatrix} \end{bmatrix} \tag{90}$$

which generates the trellis diagram illustrated in Figure 11. Note that this trellis is different than that illustrated in Figure 8 for the same rate 2/4 coded QPSK. As such, Figure 11 does not represent the optimum muiltiplicity two code.

Figure 12 illustrates the pair-state transition diagram corresponding to Figure 11 and has the transfer function

$$T(D,I)=\frac{4ac}{1-2b}$$

$$a=\frac{I}{2}\frac{\exp\left(-\frac{E_b}{N_0}\frac{4\lambda(1-2\lambda)}{1-4\lambda^2}\right)}{1-4\lambda^2}=\frac{I}{2}f(4,\lambda)$$

$$b=\frac{I}{2}\frac{\exp\left(-\frac{E_b}{N_0}\frac{2\lambda(1-2\lambda)}{1-2\lambda^2}\right)}{1-2\lambda^2}=\frac{I}{2}f(2,\lambda)$$

$$c=\frac{1}{2}\frac{\exp\left(-\frac{E_b}{N_0}\frac{2\lambda(1-2\lambda)}{1-2\lambda^2}\right)}{1-2\lambda^2}=\frac{b}{I} \qquad (91)$$

where f(x,λ) is defined in (84) with N = 2. Differentiating (91) in accordance with (86) gives the desired expression for the upper bound on bit error probability, namely,

$$P_b\le\min_{\lambda}\frac{f(4,\lambda)f(2,\lambda)}{\left(1-f(2,\lambda)\right)^2}=\min_{\lambda}\left(\frac{1-2\lambda^2}{1-4\lambda^2}\right)\frac{\exp\left(-\frac{E_b}{N_0}\frac{2\lambda(3-8\lambda^2)}{(1+2\lambda)(1-2\lambda^2)}\right)}{\left(1-2\lambda^2-\exp\left(-\frac{E_b}{N_0}\frac{2\lambda(1-2\lambda)}{(1-2\lambda^2)}\right)\right)^2} \qquad (92)$$

The upper bound on P_b of (92) is plotted in Figure 13 versus E_b/N_0.

To apply multiple symbol detection to the trellis of Figure 11, we must first convert it, in accordance with Section 8.1, to an equivalent trellis diagram with a Euclidean distance measure for all its symbols. This mathematically equivalent trellis diagram is illustrated in Figure 14 for N = 3. Figure 15 illustrates the pair-state transition diagram corresponding to Figure 14 and has the transfer function

$$T(D,I)=2c+\frac{4ab}{1-2d}$$

$$a=\frac{1}{2}(I+I^2)f(8,\lambda);\quad b=\frac{1}{4}\left[(2+I)f(4,\lambda)+If(8,\lambda)\right]$$

$$c=\frac{1}{2}If(8,\lambda);\quad d=\frac{1}{4}\left[(2I+I^2)f(8,\lambda)+I^2f(4,\lambda)\right] \qquad (93)$$

where f(x,λ) is defined in (84) with N = 3. Differentiating (93) in accordance with (86) gives the upper bound on bit error probability as

$$P_b \le \min_{\lambda} \frac{1}{2} f(8,\lambda) \left[1 + \frac{11f(4,\lambda) + 5f(8,\lambda) - 5f(4,\lambda)f(8,\lambda) + \frac{1}{2}f^2(4,\lambda) - \frac{7}{2}f^2(8,\lambda)}{2\left[1 - \frac{3}{2}f(8,\lambda) - \frac{1}{2}f(4,\lambda)\right]^2} \right] \tag{94}$$

The upper bound of (94) is superimposed on the results from (92) in Figure 13. Also included in this figure are simulation results corresponding to the exact performance of the system for N = 2 and N = 3.

We observe from Figure 13 that the curves corresponding to the Chernoff bounds of (92) and (94) are quite close to one another. The reason for this is that, for N = 3, the bound is much looser than it is for N = 2. To understand the reason for this, we compare the exact result (or its asymptotic approximation) obtained for uncoded multiple symbol DPSK with what would have been obtained by using a Chernoff bound on the pairwise error probability. In particular, if instead of the asymptotic approximation of (36) the pairwise error probability were Chernoff bounded (as has been done here in the coded case), then one would obtain a relation analogous to (61) but without the product since, for the uncoded case, the number of branches in an error event, B, is equal to one. If then one were to minimize only the exponential term in (61) with respect to λ (global minimization is difficult to accomplish in closed form), then the optimum Chernoff parameter becomes $\lambda_{opt} = 1/(N + |\delta|)$ which when substituted in the Chernoff bound gives

$$P(\underline{x} \to \hat{\underline{x}}) \le \frac{N + |\delta|}{2|\delta|} \exp\left\{ -\frac{E_s}{2N_0}(N - |\delta|) \right\} \tag{95}$$

Comparing (95) with (36), we observe that both the approximation of the exact result and the Chernoff bound yield the same exponent; however, the Chernoff bound does not produce the inverse square root of symbol energy-to-noise ratio behavior which is all important in distinguishing the performance of conventional from multiple symbol differential detection. Thus, using the Chernoff bound of (95) rather than the approximation of the exact result as in (36) to calculate the union bound on bit error probability for multiple symbol differential detection of uncoded MPSK would also result in a loose upper bound as we have observed in the coded case.

For equivalent trellis diagrams with parallel paths (as is the case in the current example - see Figure 14), we can improve upon the above as follows. Consider the terms in (82b) due to the parallel paths. Since parallel paths are one branch in length, then for these terms we can use the exact (or large SNR approximate) result for $P(\underline{x} \to \hat{\underline{x}})$ from the uncoded results in Section 3. In terms of the evaluation of P_b by the transfer function method, what we do in effect is to subtract the portion of the transfer function due to the parallel paths and apply the Chernoff bound to only the remaining portion of the transfer function. Mathematically speaking, this is equivalent to rewriting (86) as

$$P_b \le P_{b_0} + \min_{\lambda} \frac{1}{nk} \frac{d}{dI} \left[T(D,I) - T_0(D,I) \right]_{I=1} \tag{96}$$

where P_{b_0} is the portion of P_b contributed by the parallel paths; this portion is evaluated by the exact (or large SNR approximate) result, and $T_0(D,I)$ is the part of the transfer function due to these parallel paths. The amount of improvement obtained using (96) instead of (86) will be significant when the terms due to the parallel paths dominate the error probability, i.e., they yield the minimum equivalent squared Euclidean distance ($N^2 - |\delta|^2$) over all error event paths.

For the example under consideration, the term "2c" in (93) results from the parallel path in Figure 14, i.e., $T_0(D,I) = 2c$. This, in turn, contributes the term $(1/2)f(8,\lambda)$ in (94) which corresponds to the minimum equivalent squared Euclidean distance $N^2 - |\delta|^2 = 8$. Subtracting this term from (94) and replacing it by the asymptotic (large SNR) approximation [see (36)]

$$P_{b_0} \cong \frac{1}{2} \left[\frac{1}{2\sqrt{\pi \frac{E_b}{N_0}}} \left(\sqrt{\frac{N+|\delta|}{|\delta|(N-|\delta|)}} \right) \exp\left\{ -\frac{E_b}{2N_0} (N - |\delta|) \right\} \right] \tag{97}$$

where for this example, N = 3 and

$$|\delta| = \sqrt{N^2 - \left(N^2 - |\delta|^2 \right)} = \sqrt{9-8} = 1 \tag{98}$$

then, from (94), (96), and (98), we get the approximate tighter upper bound

$$P_b \le \frac{1}{2\sqrt{2\pi\frac{E_b}{N_0}}}\exp\left\{-\frac{E_b}{N_0}\right\}$$

$$+\min_{\lambda}\frac{1}{2}f(8,\lambda)\left[\frac{11f(4,\lambda)+5f(8,\lambda)-5f(4,\lambda)f(8,\lambda)+\frac{1}{2}f^2(4,\lambda)-\frac{7}{2}f^2(8,\lambda)}{2\left[1-\frac{3}{2}f(8,\lambda)-\frac{1}{2}f(4,\lambda)\right]^2}\right] \quad (99)$$

The bound of (99) is superimposed on the results in Figure 13 and is seen to yield an improvement over that corresponding to (94).

8.2 Evaluation Using the Asymptotic Approximation to Pairwise Error Probability

The upper bound of (82a) together with (81) has been evaluated for the example under consideration. In performing this evaluation, we have kept only those error event paths which yield a significant contribution to the sum. The results are also illustrated in Figure 13 and are seen to represent an improvement over the upper bounds determined in Section 8.1. However, since for this example, the trellis contains a parallel path which will dominate the error probability performance at high SNR, then the upper bound of (99) is quite close to that obtained here using the asymptotic approximation to pairwise error probability. For trellises that do not contain parallel paths, the approach leading up to Eq. (99) cannot be used and thus one must employ either the loose Chernoff bound or the asymptotic approximation method.

The same upper bound of (82a) together with (81) can also be used for conventional (N = 2) differential detection of rate 1/2 trellis coded QPSK. For the example in Section 8.1.1, the result is illustrated in Figure 13 and is again seen to agree quite well with the comparable simulation results.

8.3 Another Example

Figure 16 illustrates error probability performance results obtained by simulation for a 16 state, rate 2/3 trellis coded 8PSK using conventional (N = 2) and multiple (N = 3) symbol differential detection. This code, which is optimum on the AWGN, has the transition matrix [9: Fig. 7]

$$\mathbf{T} = \begin{bmatrix} 0 & 4 & 2 & 6 & & & & & & & & & & & & \\ & & & & 1 & 5 & 3 & 7 & & & & & & & & \\ & & & & & & & & 4 & 0 & 6 & 2 & & & \\ & & & & & & & & & & & & 5 & 1 & 7 & 3 \\ 2 & 6 & 0 & 4 & & & & & & & & & & & & \\ & & & & 3 & 7 & 1 & 5 & & & & & & & & \\ & & & & & & & & 6 & 2 & 4 & 0 & & & & \\ & & & & & & & & & & & & 7 & 3 & 5 & 1 \\ 4 & 0 & 6 & 2 & & & & & & & & & & & & \\ & & & & 5 & 1 & 7 & 3 & & & & & & & & \\ & & & & & & & & 0 & 4 & 2 & 6 & & & & \\ & & & & & & & & & & & & 1 & 5 & 3 & 7 \\ 6 & 2 & 4 & 0 & & & & & & & & & & & & \\ & & & & 7 & 3 & 5 & 1 & & & & & & & & \\ & & & & & & & & 2 & 6 & 0 & 4 & & & & \\ & & & & & & & & & & & & 3 & 7 & 1 & 5 \end{bmatrix} \qquad (100)$$

We observe from this figure that in going from N = 2 to N = 3, an improvement in E_b/N_0 performance of about 0.75 dB is obtained for the range of bit error probabilities illustrated.

9.0 Conclusions

We have demonstrated a multiple symbol differential detection technique for MPSK which is based on maximum-likelihood sequence estimation (MLSE) of the transmitted phases rather than symbol-by-symbol detection. The performance of this multiple symbol scheme fills the gap between ideal coherent and differentially coherent detection of MPSK. The amount of improvement gained over differentially coherent detection (two symbol observation interval per decision) depends on the number of additional symbol intervals added to the observation. In the limit as the observation interval approaches infinity, the performance approaches that of ideal coherent detection with differential encoding. Practically, this limiting performance is approached with observation times (decision memory) only on the order of a few additional symbol intervals. Thus, even in situations (e.g., benign environments) where one would ordinarily not turn to differential detection, it might now be desirable to employ multiple symbol differential detection for reasons related to simplicity of implementation. For

example, the acquisition and maintenance of a locked carrier tracking loop as required in a coherent detection system is not needed here.

As for the uncoded case, the use of multiple symbol differential detection of trellis coded MPSK can also offer an improvement in error probability performance over conventional (two-symbol observation) differential detection of the same coded modulation. Again only a slight increase in the length of the observation interval is necessary to demonstrate a significant improvement.

10.0 References

[1] Lawton, J.G., "Investigation of Digital Data Communication Systems," Report No. UA-1420-S-1, Cornell Aeronautical Laboratory, Inc., Buffalo, NY, January 3, 1961. Also available as ASTIA Document No. 256 584.

[2] Lindsey, W.C. and Simon, M.K., *Telecommunication Systems Engineering*, Prentice-Hall, Englewood Cliffs, NJ, 1973.

[3] Stein, S., "Unified Analysis of Certain Coherent and Noncoherent Binary Communication Communications Systems," IEEE Transactions on Information Theory, January, 1964, pp. 43-51.

[4] Marcum, J., "Tables of Q Functions," RAND Corporation Report M-339, January, 1950.

[5] M. Schwartz, W.R. Bennett, and S. Stein, Communication Systems and Techniques, McGraw-Hill, Inc., New York, 1966.

[6] C.W. Helstrom, Statistical Theory of Signal Detection, Pergamon Press, p. 164.

[7] D. Divsalar, M.K. Simon, "Multiple Trellis Coded Modulation (MTCM)," JPL Publication 86-44 (MSAT-X Report No. 141), November 15, 1986. Also in IEEE Transactions on Communications, Vol. 36, No. 4, April 1988, pp. 410-419.

[8] M.K. Simon, D. Divsalar, "The Performance of Trellis Coded Multilevel DPSK on a Fading Mobile Satellite Channel," JPL Publication 87-8 (MSAT-X Report No. 144), June 1, 1987. Also in IEEE Transactions on Vehicular Technology, Vol. 37, No. 2, May 1988, pp. 78-91.

[9] G. Ungerboeck, "Channel Coding with Multilevel/Phase Signals," IEEE Transactions on Information Theory, Vol, IT-28, No. 1, January 1982, pp. 55-67.

[10] J. G. Proakis, Digital Communications, McGraw-Hill Book Co., New York, NY, 1983.

[11] M.K. Simon, J.K. Omura, R.A. Scholtz, and B.K. Levitt, Spread Spectrum Communications, Vol. 1, Computer Science Press, Rockville, MD, 1985, pp. 248-249.

[12] M. Schwartz, W.R. Bennett, and S. Stein, Communication Systems and Techniques, McGraw-Hill, Inc., New York, NY, 1966.

[13] L. Hormander, The Analysis of Linear Partial Differenital Operators, Vol. I, Springer-Verlag, New York, NY, 1983.

[14] D. Divsalar, "Performance of Mismatched Receivers on Bandlimited Channels," Ph.D. Dissertation, University of California, Los Angeles, CA, 1978.

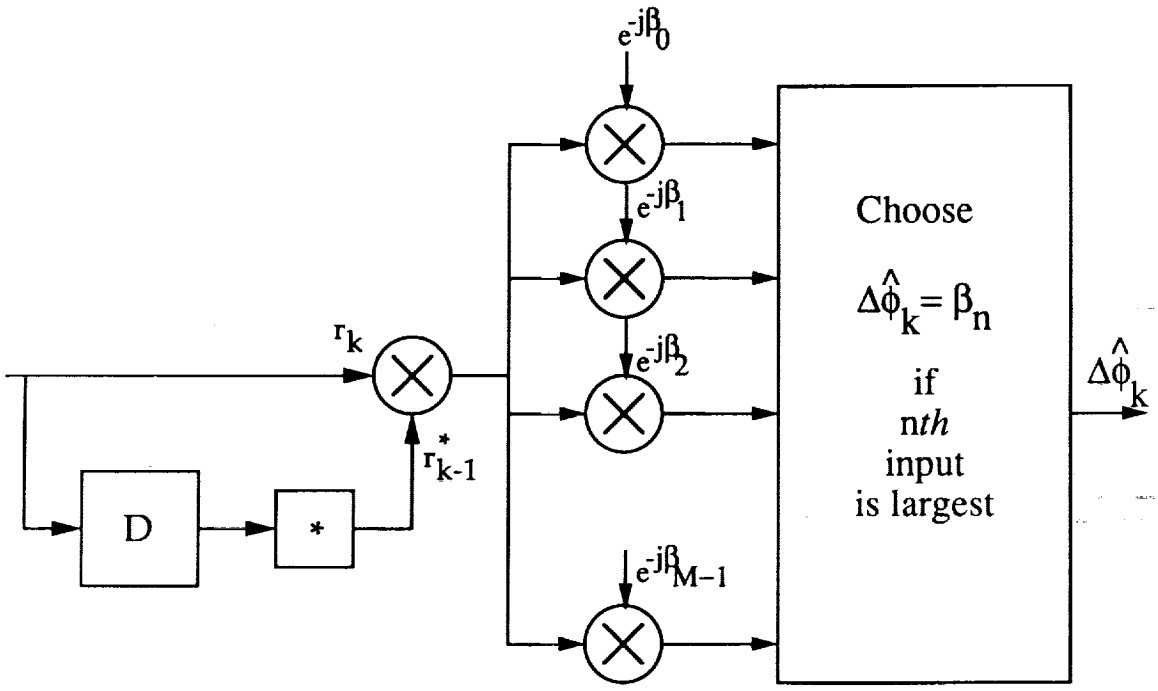

Figure 1. Conventional Differential Detector for MPSK

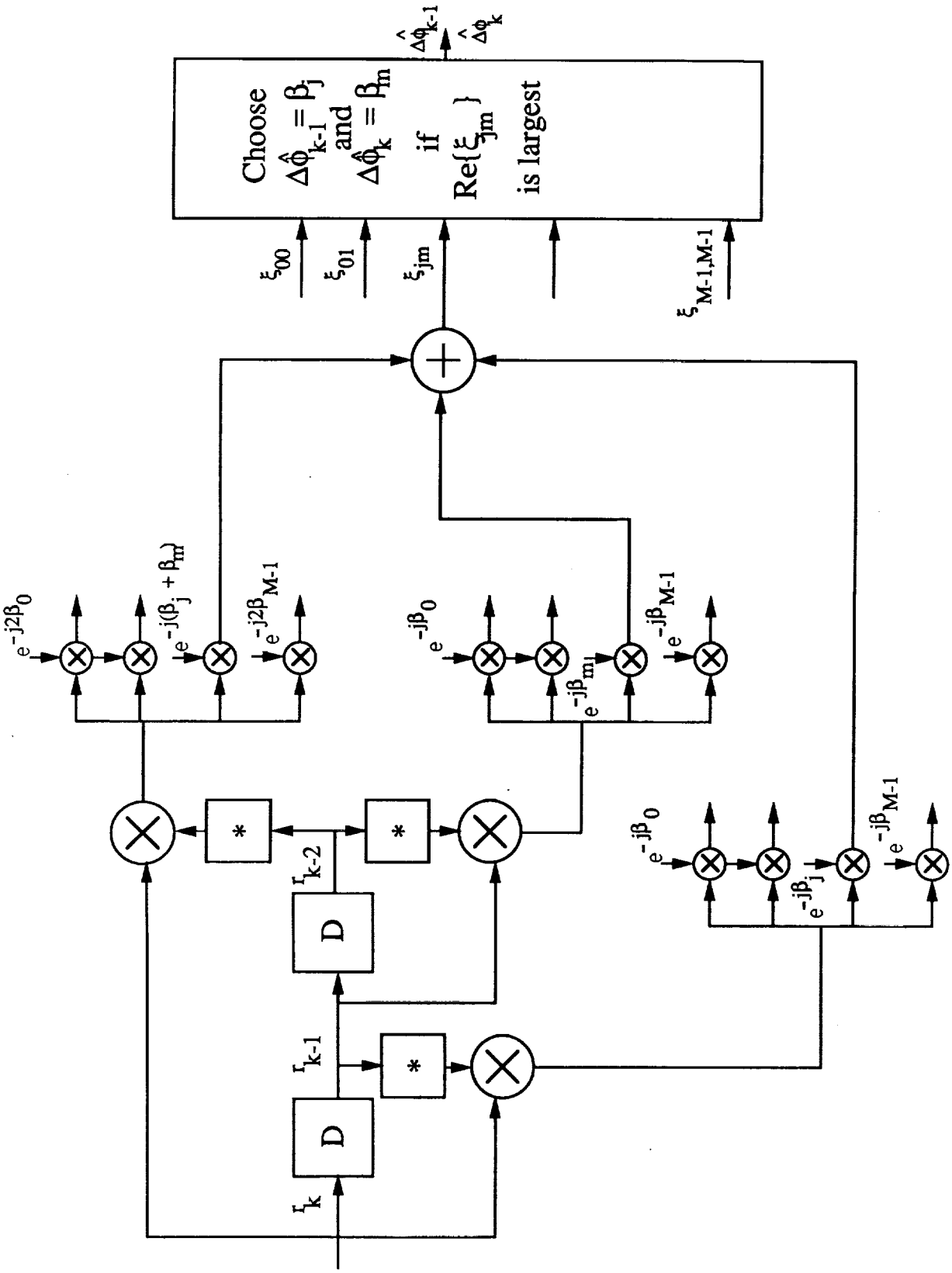

Figure 2. Parallel Implementation of Multiple Bit Differential Detector; N=3

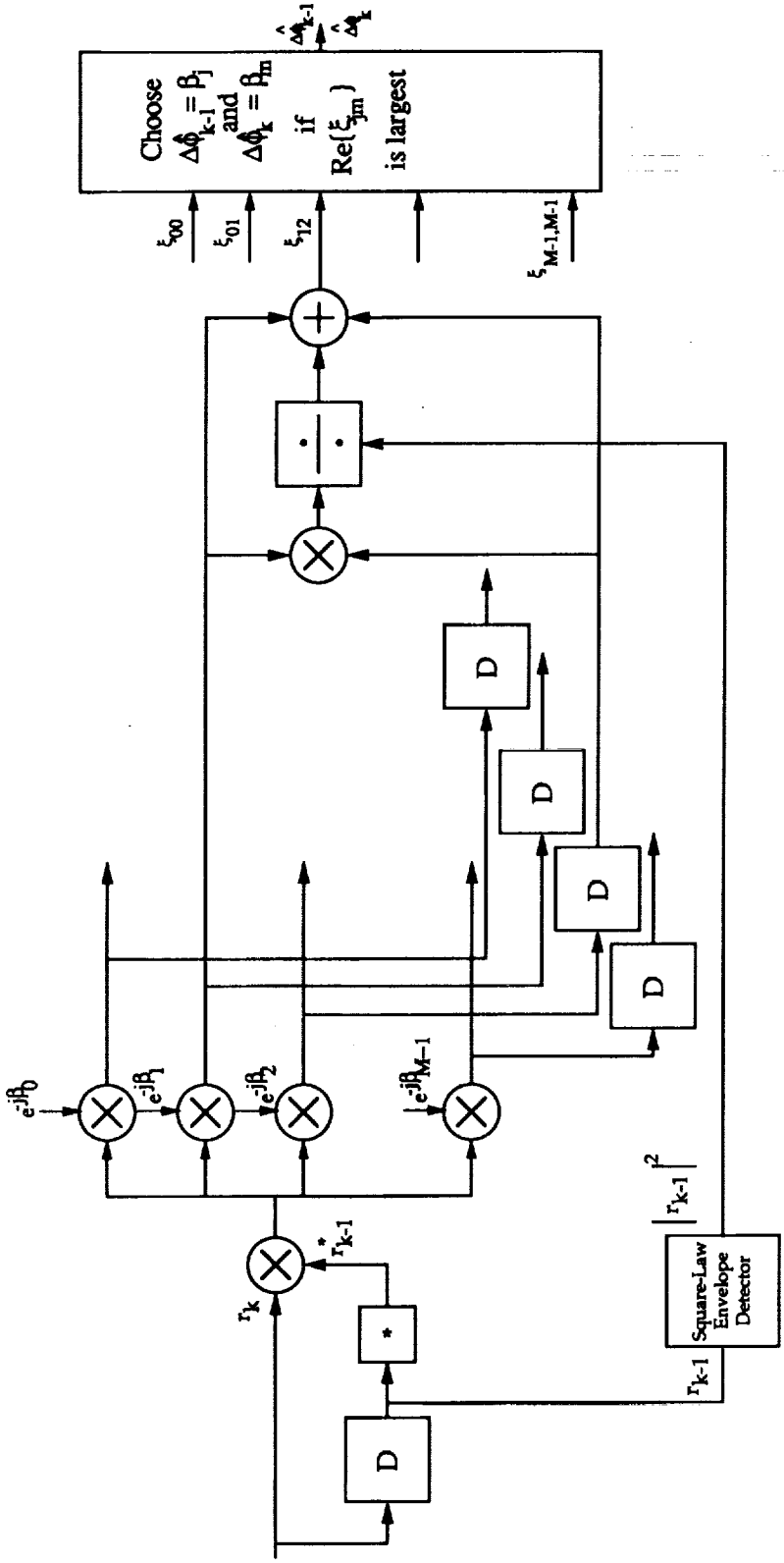

Figure 3. Serial Implementation of Multiple Bit Differential Detector; N=3

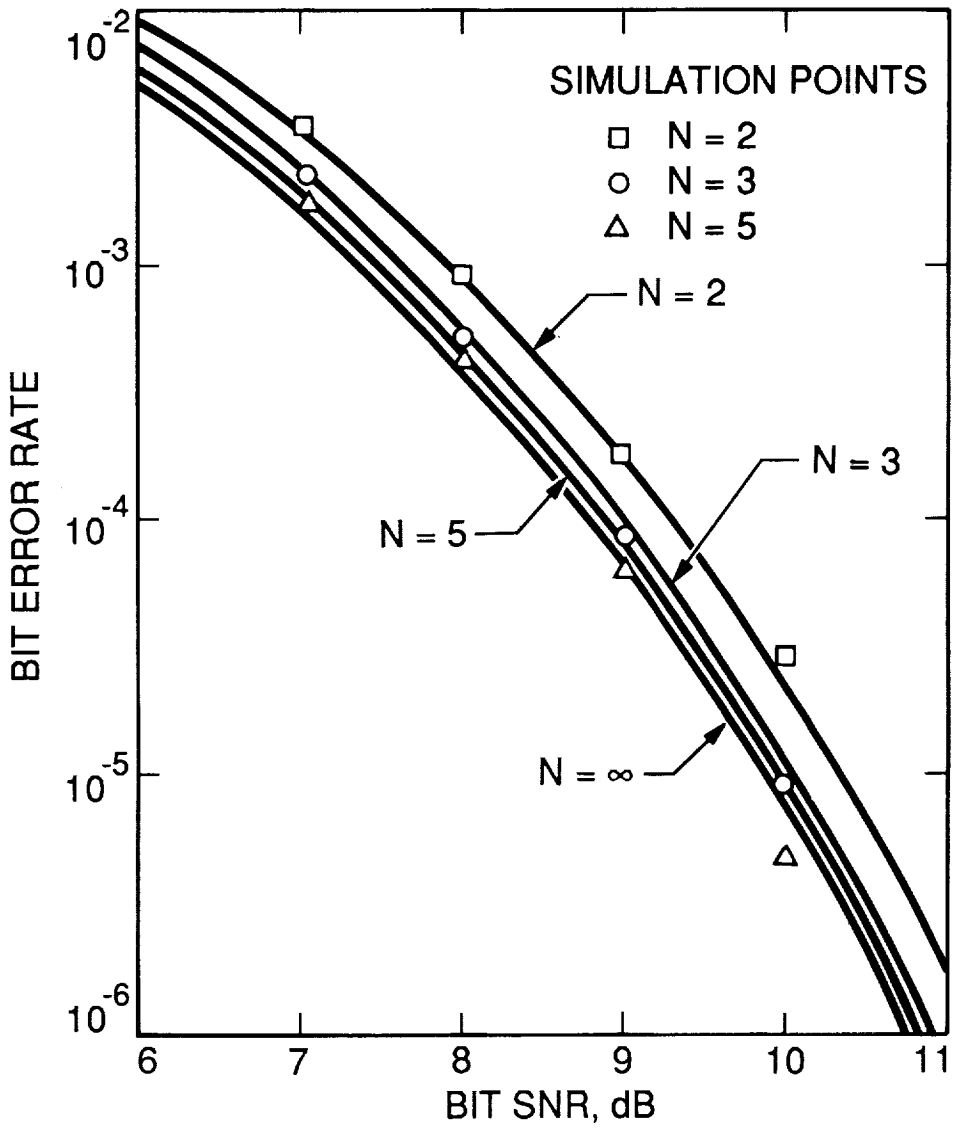

Figure 4. Bit Error Probability Versus E_b/N_0 for Multiple Differential Detection of MPSK; M=2

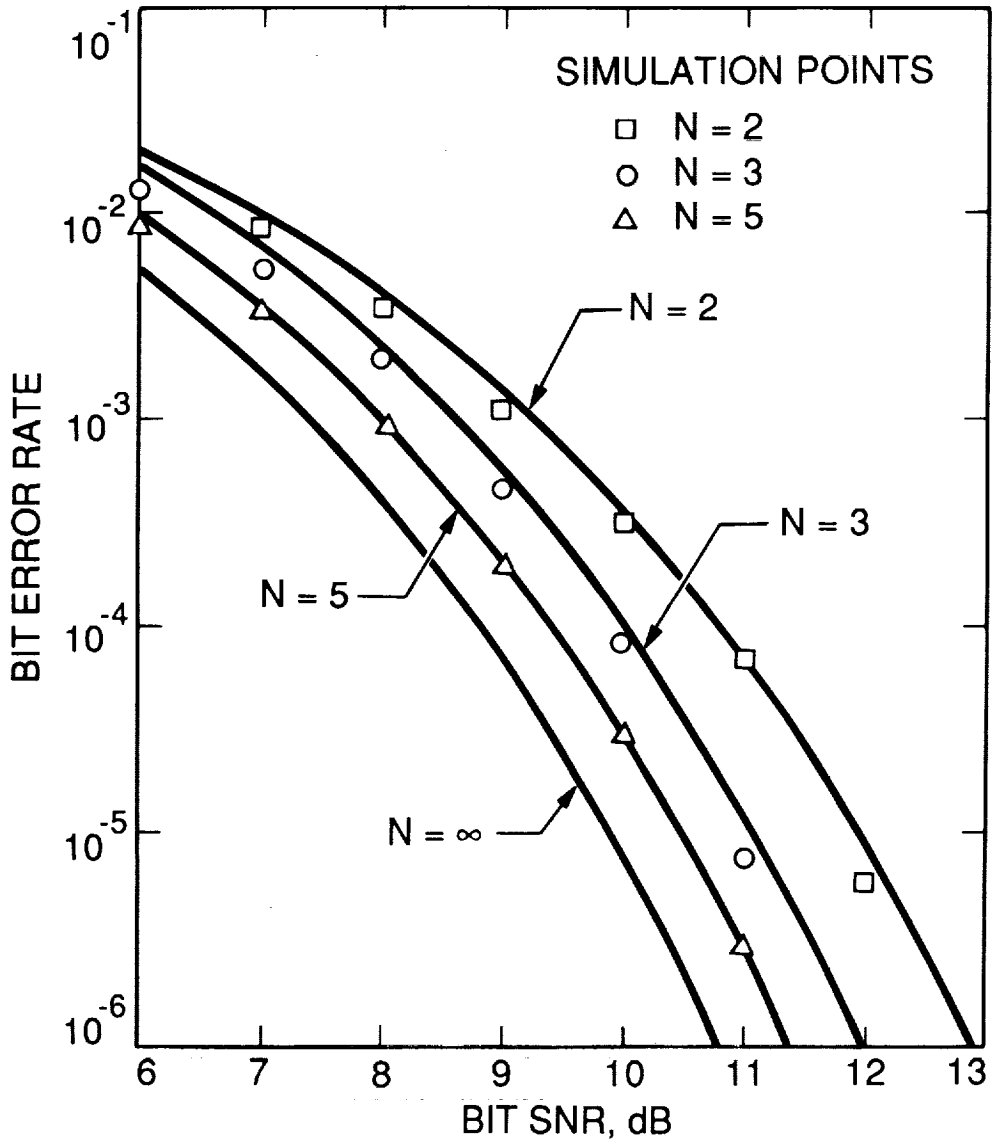

Figure 5. Bit Error Probability Versus E_b/N_0 for Multiple Differential Detection of MPSK; M=4

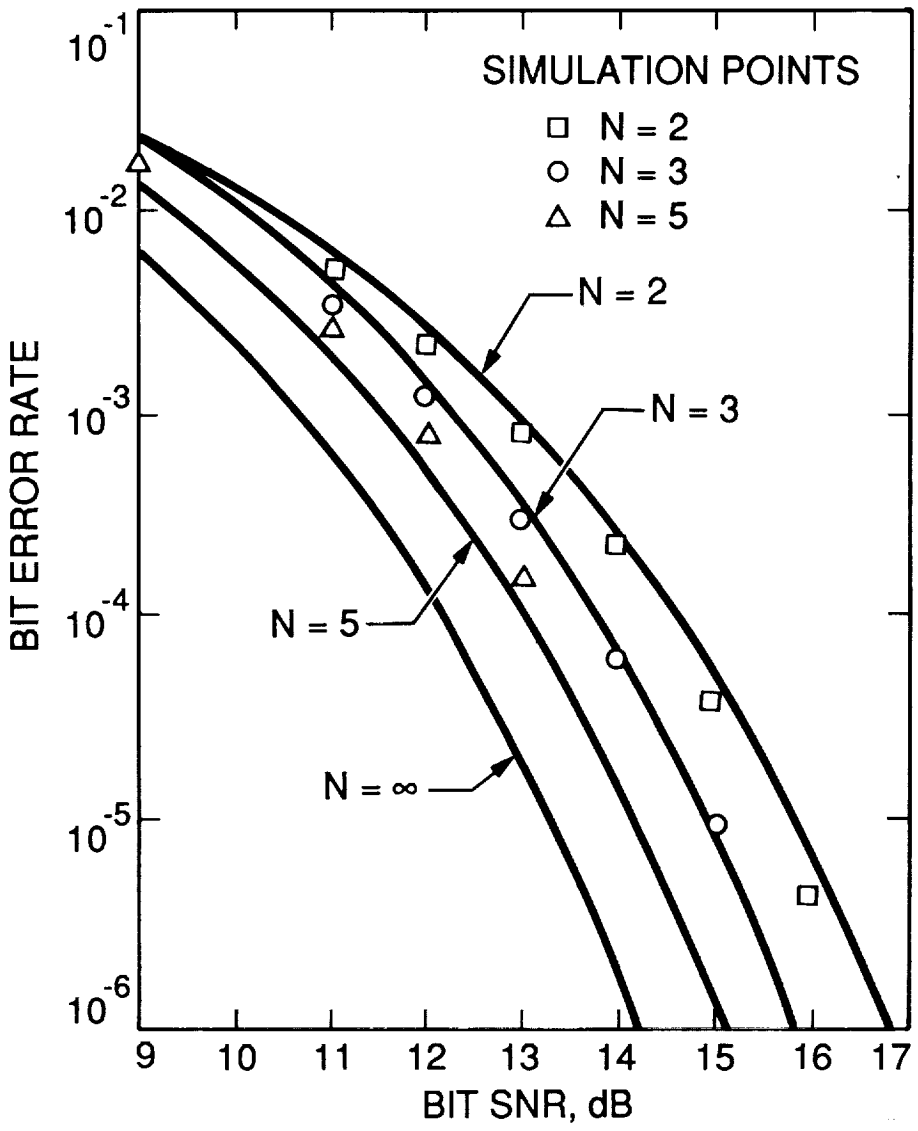

Figure 6. Bit Error Probability Versus E_b/N_0 for Multiple Differential Detection of MPSK; M=8

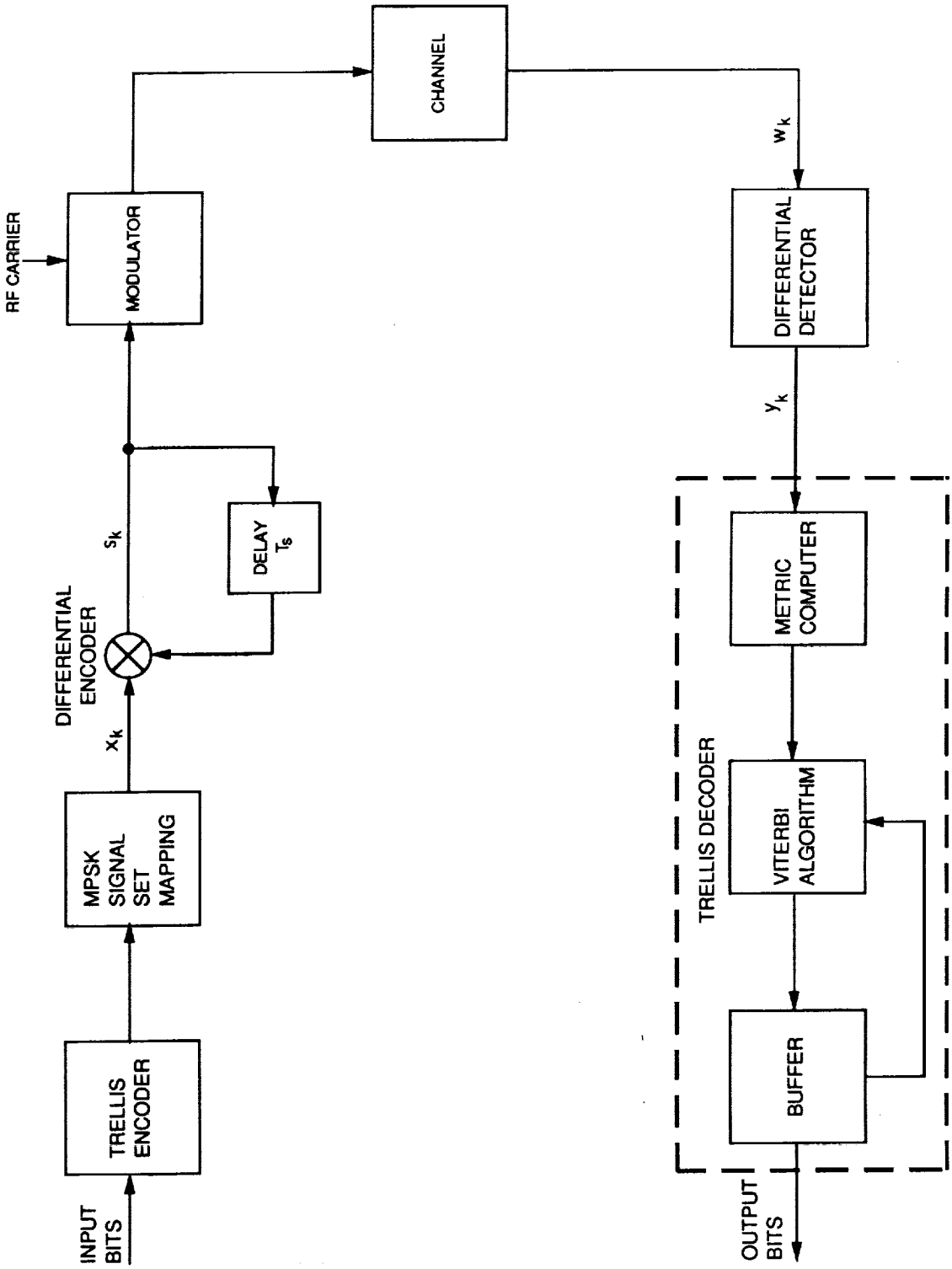

Figure 7. Block Diagram of the Trellis Coded MDPSK System

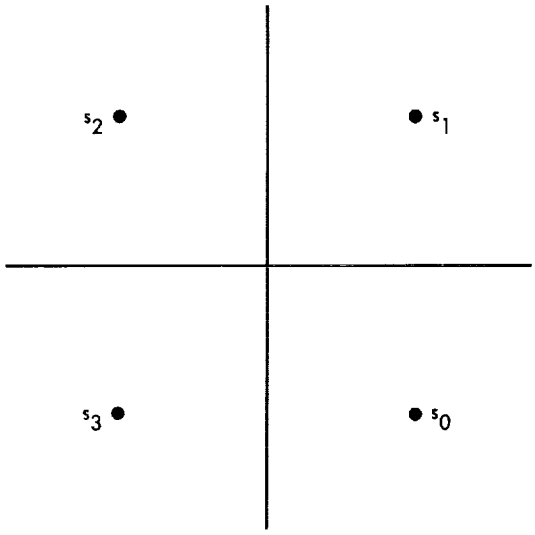

SYMMETRIC 4-PSK

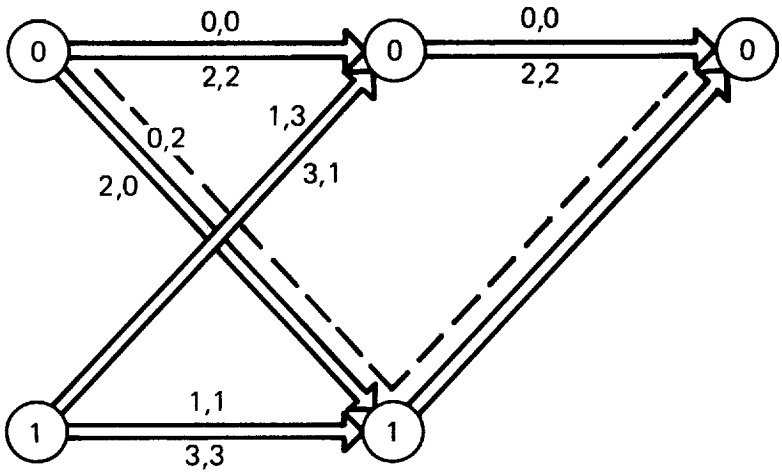

Figure 8. QPSK Signal Constellation and Trellis Diagram for Optimum Rate 2/4 Multiple Trellis Coded QPSK

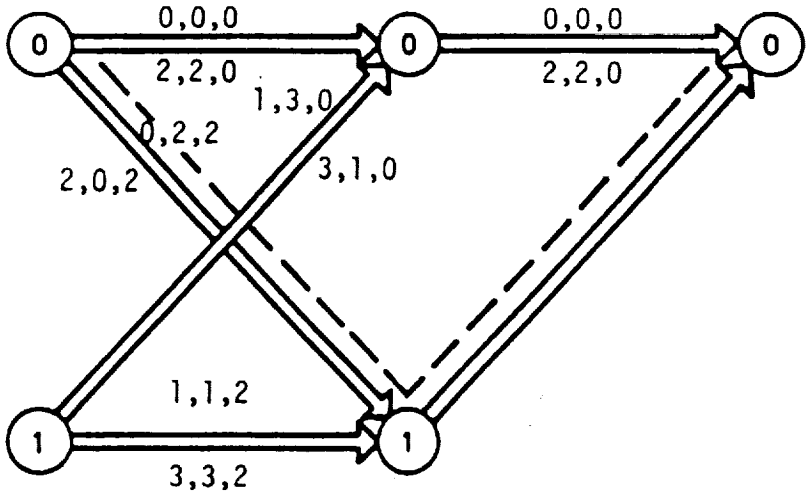

Figure 9. Trellis With Squared Euclidean Distance Measure That is Mathematically Equivalent to Figure 8

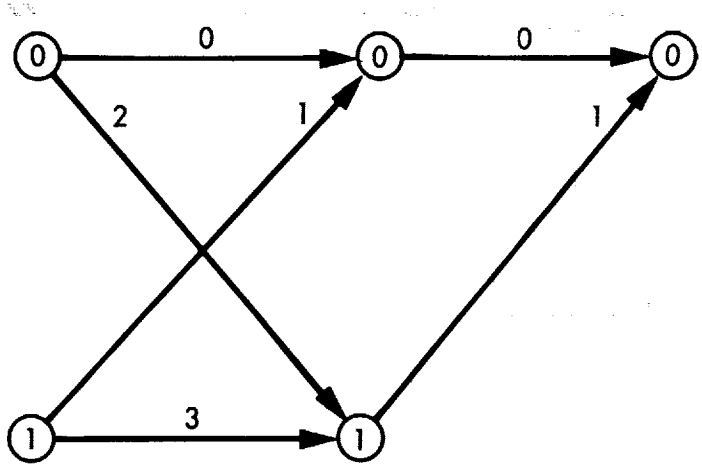

Figure 10. Trellis Diagram for Conventional Rate 1/2 Trellis Coded QPSK

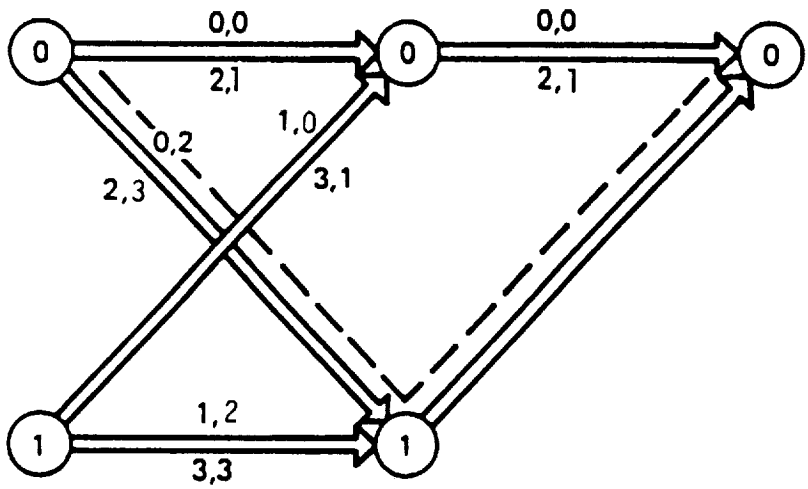

Figure 11. Trellis Diagram for Rate 2/4 Multiple Trellis Coded QPSK Equivalent to Figure 10

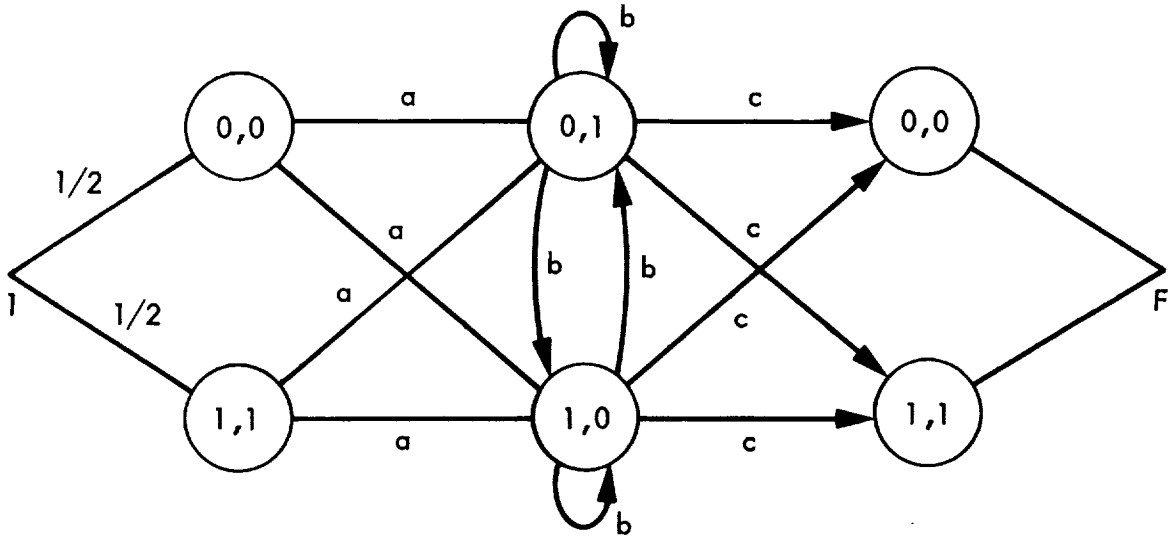

Figure 12. Pair-State Transition Diagram for Trellis Diagram of Figure 11

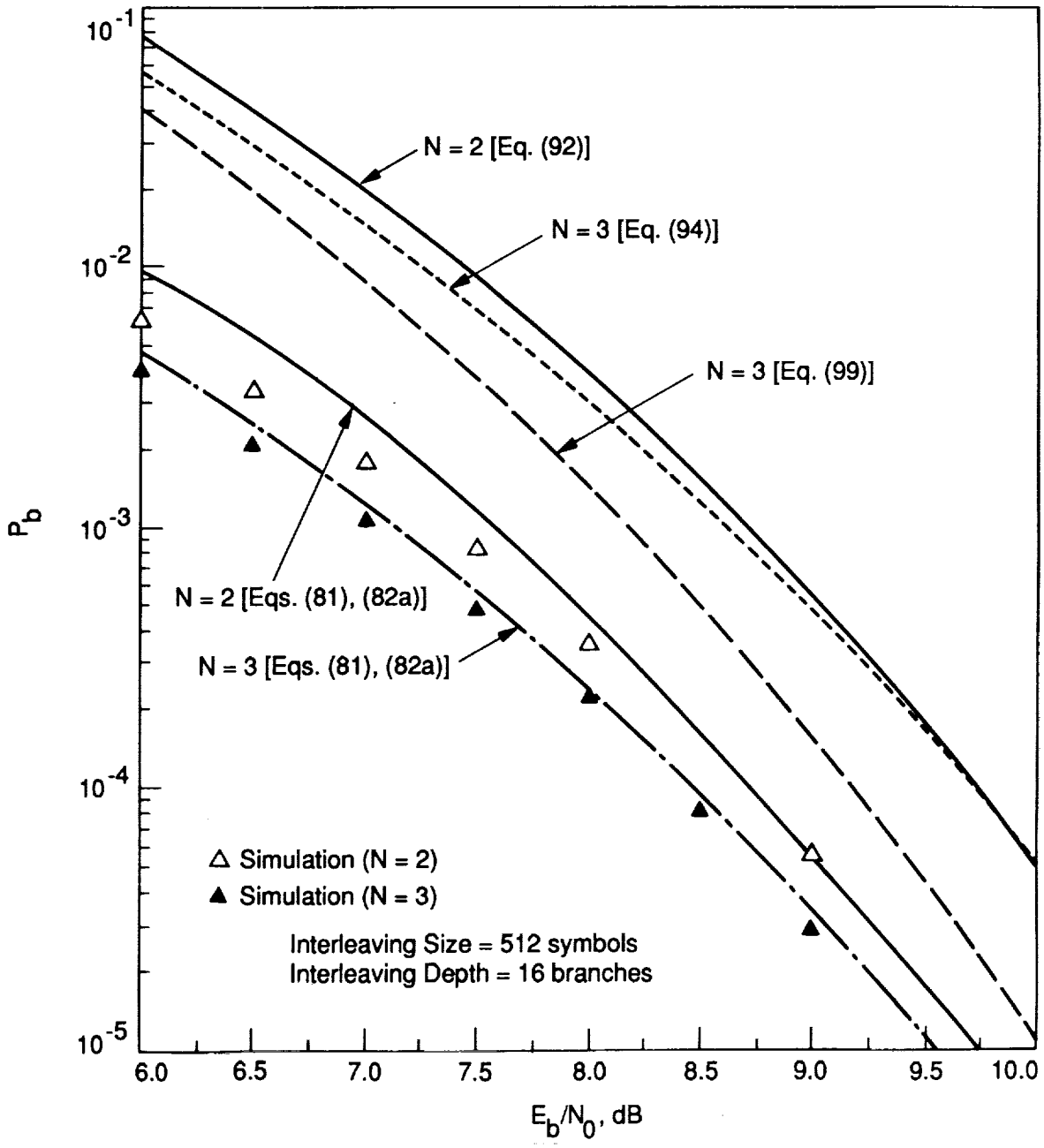

Figure 13. Analytical and Simulation Results for Bit Error Probability of 2-State, Rate 1/2 Trellis Coded QPSK With Conventional (N=2) and Multiple (N=3) Symbol Differential Detection

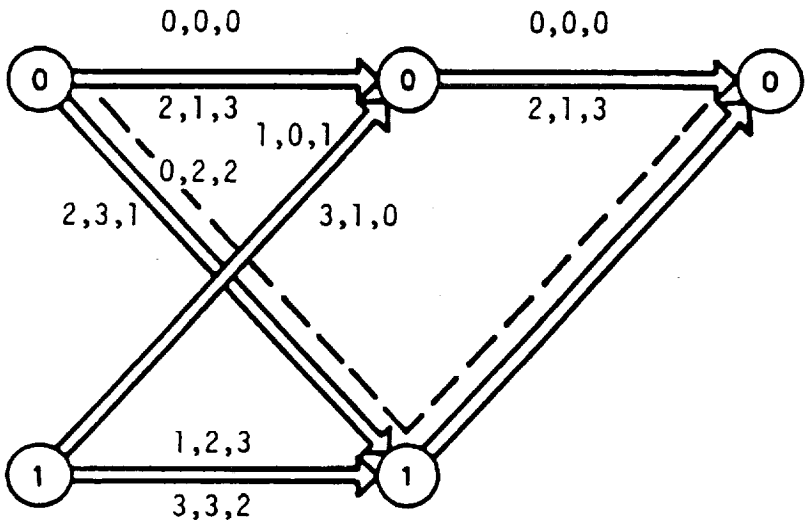

Figure 14. Trellis With Squared Euclidean Distance Measure That is Mathematically Equivalent to Figure 11

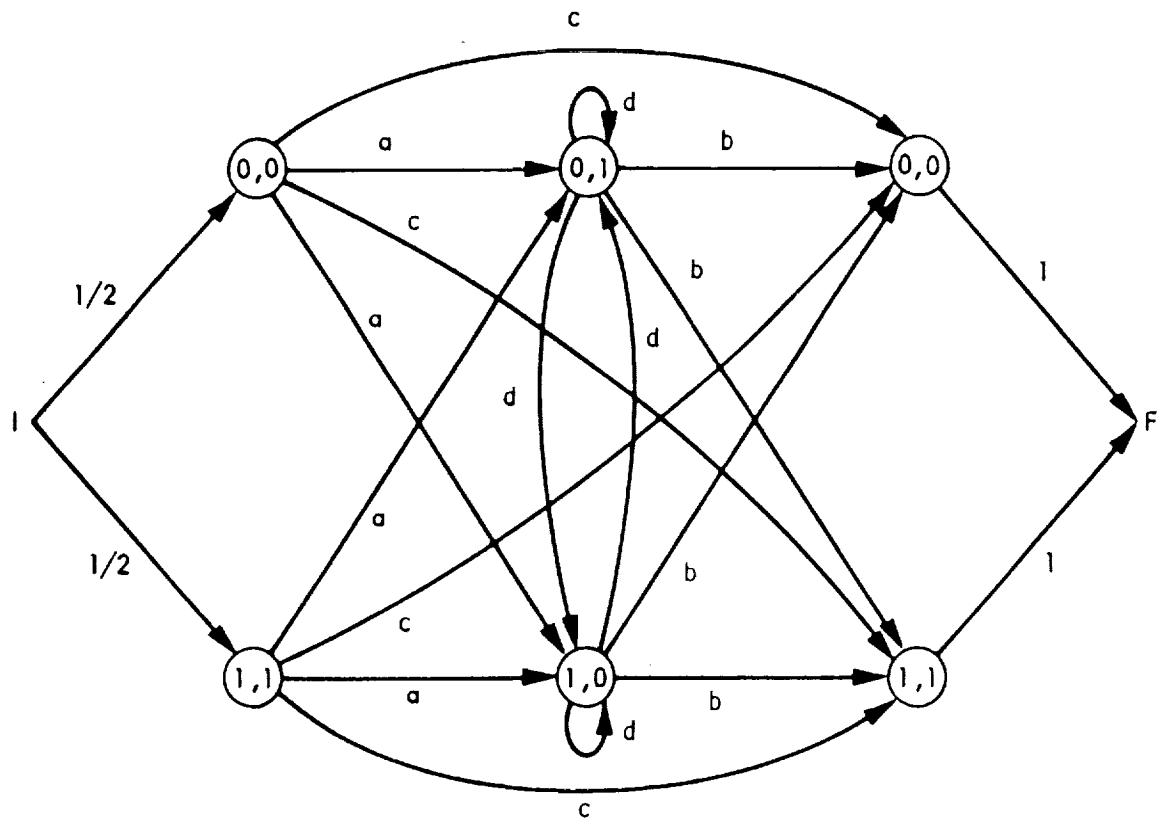

Figure 15. Pair-State Transition Diagram for Trellis Diagram of Figure 14

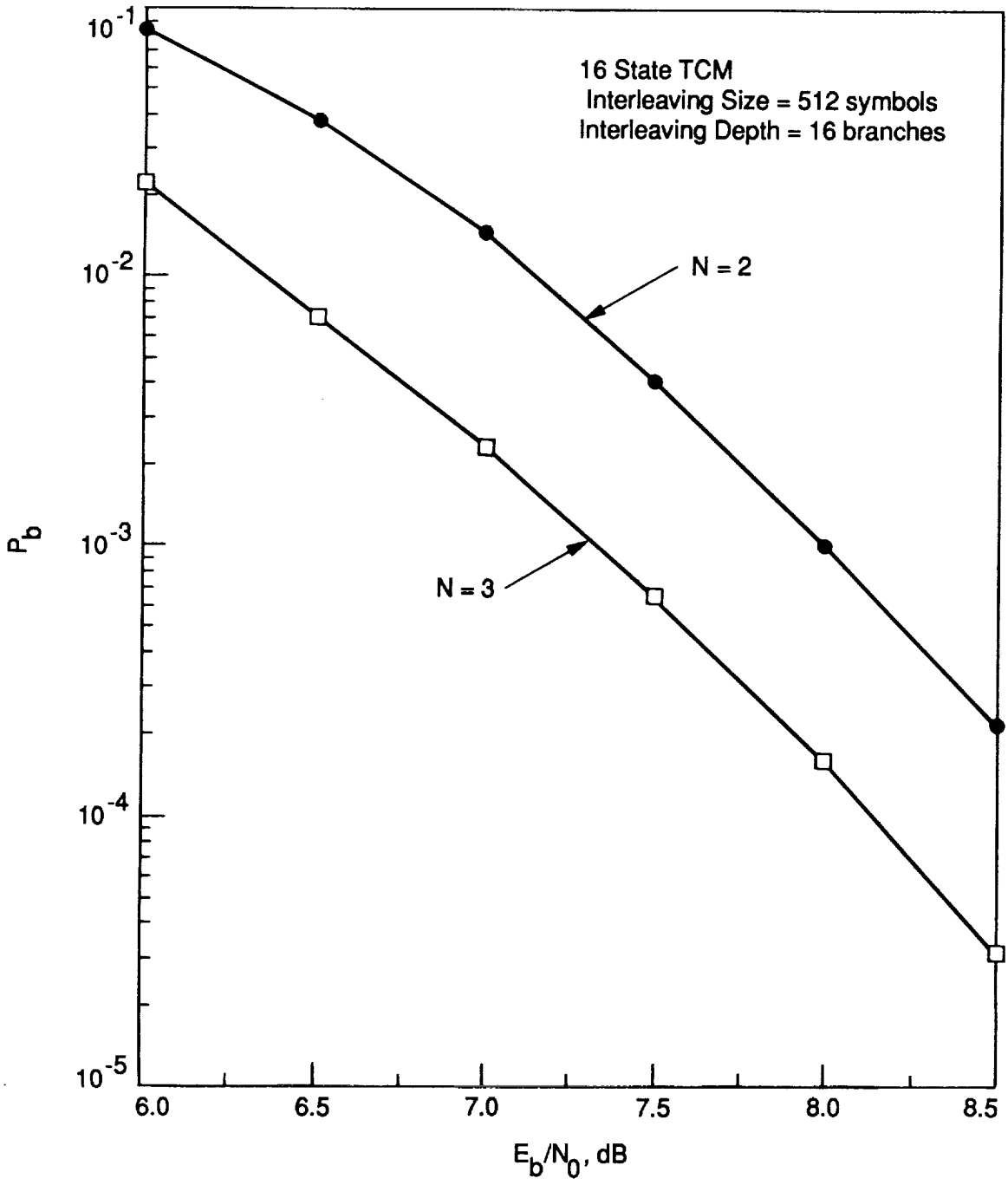

Figure 16. Simulation Results for Bit Error Probability of 16 State, Rate 2/3 Trellis Coded 8PSK With Conventional (N=2) and Multiple (N=3) Symbol Differential Detection

Appendix A

Evaluation of the Pairwise Error Probability

In [3], it is shown that for complex Gaussian random variables z_1 and z_2 with identical variances and arbitrary means and covariance, the pairwise probability of error $\Pr\{|z_2|^2 > |z_1|^2\}$ is given by

$$\Pr\{|z_2|^2 > |z_1|^2\} = \frac{1}{2}\left[1 - Q(\sqrt{b},\sqrt{a}) + Q(\sqrt{a},\sqrt{b})\right] \tag{A-1}$$

where $Q(\alpha,\beta)$ is Marcum's Q-function [4] and

$$\left\{\begin{matrix} b \\ a \end{matrix}\right\} = \frac{1}{2N_s}\left\{\frac{S_1 + S_2 - 2|\rho|\sqrt{S_1 S_2}\cos(\theta_1 - \theta_2 + \phi)}{1-|\rho|^2} \pm \frac{S_1 - S_2}{\sqrt{1-|\rho|^2}}\right\} \tag{A-2}$$

with

$$\begin{aligned} S_1 &\triangleq \frac{1}{2}|\overline{z_1}|^2; \quad S_2 \triangleq \frac{1}{2}|\overline{z_2}|^2 \\ N_s &\triangleq \frac{1}{2}\overline{|z_1 - \overline{z_1}|^2} = \frac{1}{2}\overline{|z_2 - \overline{z_2}|^2} \\ \rho &\triangleq \frac{1}{2N_s}\overline{(z_1 - \overline{z_1})^*(z_2 - \overline{z_2})} \\ \phi &= \arg\{\rho\}; \quad \theta_1 = \arg\{\overline{z_1}\}; \quad \theta_2 = \arg\{\overline{z_2}\} \end{aligned} \tag{A-3}$$

Here we associate z_1 and z_2 with $w(\underline{\Delta\phi})$ and $w(\underline{\Delta\hat{\phi}})$, respectively, of (23).

Using (1) and (2) in (A-3), we get

$$\begin{aligned} \overline{z_1} &= \sqrt{2P}\sum_{i=0}^{N-1} e^{j\phi_{k-i}} e^{-j\sum_{m=0}^{N-i-2}\Delta\phi_{k-i-m}} = \sqrt{2P}e^{j\phi_{k-N+1}}N \\ \overline{z_2} &= \sqrt{2P}\sum_{i=0}^{N-1} e^{j\phi_{k-i}} e^{-j\sum_{m=0}^{N-i-2}\Delta\hat{\phi}_{k-i-m}} = \sqrt{2P}e^{j\phi_{k-N+1}}\delta \end{aligned} \tag{A-4}$$

where

$$\delta \overset{\Delta}{=} \sum_{i=0}^{N-1} e^{\,j \sum_{m=0}^{N-i-2} \left(\Delta\phi_{k-i-m} - \Delta\hat{\phi}_{k-i-m}\right)} \tag{A-5}$$

where it is understood that the summation equals zero if the upper summation index is negative. Substituting (A-4) into (A-3), gives

$$S_1 = PN^2; \quad S_2 = P|\delta|^2 \tag{A-6}$$

Also, using (3)

$$N_z = \frac{1}{2} E\left\{ \left| \sum_{i=0}^{N-1} n_{k-i} e^{\,-j \sum_{m=0}^{N-i-2} \Delta\phi_{k-i-m}} \right|^2 \right\} = \frac{NN_0}{T} \tag{A-7}$$

and

$$\rho = \frac{1}{2N_z} \sum_{i=0}^{N-1} \sum_{n=0}^{N-1} E\left\{ n_{k-i} n_{k-n}^{*} \right\} e^{\,j\left(\sum_{m=0}^{N-i-2} \Delta\phi_{k-i-m} - \sum_{m=0}^{N-n-2} \Delta\hat{\phi}_{k-n-m} \right)}$$

$$= \frac{1}{2N_z} \sum_{i=0}^{N-1} \frac{2N_0}{T} e^{\,j\left(\sum_{m=0}^{N-i-2} \Delta\phi_{k-i-m} - \Delta\hat{\phi}_{k-i-m} \right)} = \frac{\delta}{N} \tag{A-8}$$

Finally, substituting (A-6) - (A-8) into (A-1) gives the desired result, namely,

$$\Pr\left\{ \hat{\eta} > \eta | \underline{\Delta\phi} \right\} = \frac{1}{2}\left[1 - Q(\sqrt{b}, \sqrt{a}) + Q(\sqrt{a}, \sqrt{b}) \right] \tag{A-9}$$

where

$$\begin{Bmatrix} b \\ a \end{Bmatrix} = \frac{E_s}{2N_0}\left[N \pm \sqrt{N^2 - |\delta|^2} \right] \tag{A-10}$$

where E_S = PT is the energy per data symbol.

Appendix B

Proof of Eqs. (42) and (48)

Starting with the definition of δ in (27), we now write it in the form

$$\delta = 1 + \sum_{i=1}^{N-1} e^{j\alpha_i} \tag{B-1}$$

where

$$\alpha_i \overset{\Delta}{=} \sum_{n=1}^{i} \delta\phi_{k-N+1+n} \tag{B-2}$$

Thus, δ is the sum of N unit vectors the first of whose arguments is zero and the rest of whose arguments are increasingly larger sums of the phase errors in accordance with (B-2). Note that the values of the accumulated phase errors, α_i's, also range over the set $\pm 2\pi m/M$; m = 0 ,1, ..., M/2 - 1. We are interested in determining the various possible solutions for the δφ's such that the maximum value of the magnitude of δ, namely $|\delta|_{max}$ of (49) is achieved.

For arbitrary M, there are four situations that achieve $|\delta|_{max}$. We shall refer to these as cases 1, 2, 3, and 4 which are described as follows.

Case 1: All N-1 vectors $e^{j\alpha_i}$; i = 1, 2, ..., N-1 must be collinear and equal to $e^{j2\pi/M}$. Thus, $\alpha_i = 2\pi/M$; i = 1, 2, ..., N-1 which, in accordance with (B-2), has the single solution

$$\delta\phi_{k-N+2} = \frac{2\pi}{M}; \quad \delta\phi_{k-N+i} = 0; i = 3,4,\ldots,N \tag{B-3}$$

Case 2: All N-1 vectors $e^{j\alpha_i}$; i = 1, 2, ..., N-1 must be collinear and equal to $e^{-j2\pi/M}$. Thus, $\alpha_i = -2\pi/M$; i = 1, 2, ..., N-1 which, in accordance with (B-2), has the single solution

$$\delta\phi_{k-N+2} = -\frac{2\pi}{M}; \quad \delta\phi_{k-N+i} = 0; i = 3,4,\ldots,N \tag{B-4}$$

Case 3: Any N-2 vectors $e^{j\alpha_i}$ must be collinear and equal to $e^{j0} = 1$ and the remaining vector must be equal to $e^{j2\pi/M}$. For this case there are N-1 different solutions. For example, suppose first that $\alpha_1 = 2\pi/M$, and $\alpha_i = 0$; i = 2, 3, ..., N-1. Then,

$$\delta\phi_{k-N+2} = \frac{2\pi}{M}; \quad \delta\phi_{k-N+3} = -\frac{2\pi}{M}; \quad \delta\phi_{k-N+i} = 0; i = 4,5,\ldots,N \tag{B-5}$$

Next, let $\alpha_2 = 2\pi/M$, and $\alpha_i = 0$; i = 1, 3, 4, ..., N-1. Then,

$$\delta\phi_{k-N+3} = \frac{2\pi}{M}; \quad \delta\phi_{k-N+4} = -\frac{2\pi}{M}; \quad \delta\phi_{k-N+i} = 0; i = 2,5,6,\ldots,N \tag{B-6}$$

In general for $\alpha_\ell = 2\pi/M$, $\ell = 1, 2, \ldots, N-2$ and $\alpha_i = 0$; i = 1, 2, ..., N-1; $i \neq \ell$, we have the solution

$$\delta\phi_{k-N+\ell+1} = \frac{2\pi}{M}; \quad \delta\phi_{k-N+\ell+2} = -\frac{2\pi}{M}; \quad \delta\phi_{k-N+i} = 0; i = 1,2,\ldots\ell,\ell+3,\ldots,N \tag{B-7}$$

Finally, for $\alpha_{N-1} = 2\pi/M$ and $\alpha_i = 0$; i = 1, 2, ..., N-2, the solution is

$$\delta\phi_k = \frac{2\pi}{M}; \quad \delta\phi_{k-N+i} = 0; i = 1,2,\ldots,N-1 \tag{B-8}$$

Case 4: Any N-2 vectors $e^{j\alpha_i}$ must be collinear and equal to $e^{j0} = 1$ and the remaining vector must be equal to $e^{-j2\pi/M}$. For this case there are again N-1 different solutions which are identical to those described by (B-5) to (B-8) with $2\pi/M$ replaced by $-2\pi/M$ and vice versa.

We note that for cases 3 and 4, N-2 of the solutions are characterized by having one $\delta\phi = 2\pi/M$, one $\delta\phi = -2\pi/M$, and the rest of the $\delta\phi$'s equal to zero. The remaining solution has one $\delta\phi = 2\pi/M$ and the rest of the $\delta\phi$'s equal to zero.

To compute the accumulated Hamming distance of (47), where $w(\underline{u},\underline{\hat{u}})$ corresponds only to those error sequences that result in $|\delta|_{max}$, we proceed as follows. We assume a Gray code bit to symbol assignment where $\delta\phi = \pm 2\pi/M$ corresponds to an adjacent phase symbol error and thus a single bit error or a Hamming distance equal to 1. Also, a value $\delta\phi = 0$ implies no

symbol error or a Hamming distance equal to zero. Thus, the following accumulated Hamming distances occur for each of the four cases.

Case 1:

$$w(\underline{u},\hat{\underline{u}}) = 1 \tag{B-9}$$

Case 2:

$$w(\underline{u},\hat{\underline{u}}) = 1 \tag{B-10}$$

Case 3:

$$w(\underline{u},\hat{\underline{u}}) = (2)(N-2) + (1)(1) = 2(N-2) + 1 \tag{B-11}$$

Case 4:

$$w(\underline{u},\hat{\underline{u}}) = (2)(N-2) + (1)(1) = 2(N-2) + 1 \tag{B-12}$$

Finally, the accumulated Hamming distance is obtained by summing (B-9) through (B-12) which yields (for N > 2)

$$\sum_{\underline{\Delta\phi} \neq \underline{\Delta\hat{\phi}}} w(\underline{u},\hat{\underline{u}}) = 4(N-1) \tag{B-13}$$

which agrees with (48).

For N = 2, Cases 3 and 4 do not occur since N - 2 = 0. Thus, the accumulated Hamming distance is merely the sum of (B-9) and (B-10) which yields

$$\sum_{\underline{\Delta\phi} \neq \underline{\Delta\hat{\phi}}} w(\underline{u},\hat{\underline{u}}) = 2 \tag{B-14}$$

in agreement with (47).

For M=2, $e^{j2\pi/M} = e^{j\pi} = e^{-j2\pi/M}$ and thus cases 1 and 2 are one and the same and similarly for cases 3 and 4. Thus, for binary multiple bit DPSK, we have only *half* the solutions in which case (B-13) becomes

$$\sum_{\underline{\Delta\phi}\neq\underline{\Delta\hat{\phi}}} w(\underline{u},\underline{\hat{u}}) = \begin{cases} 2(N-1); & N>2 \\ 1; & N=2 \end{cases} \tag{B-15}$$

which agrees with (42). Q.E.D.

Appendix C

Evaluation of the Chernoff Bound on Pairwise Error Probability

Here we derive an upper Chernoff bound on the pair-wise error probability $\Pr\left\{\sum_{i=1}^{B}\hat{\eta}_i > \sum_{i=1}^{B}\eta_i \middle| \underline{\Delta\phi}\right\}$. In particular, from the definition of the Chernoff bound [11]

$$\Pr\left\{\sum_{i=1}^{B}\hat{\eta}_i > \sum_{i=1}^{B}\eta_i \middle| \underline{\Delta\phi}\right\} \le E\left\{e^{\lambda_0\left(\sum_{i=1}^{B}\hat{\eta}_i - \sum_{i=1}^{B}\eta_i\right)} \middle| \underline{\Delta\phi}\right\} = \prod_{\substack{i=1 \\ \underline{\Delta\hat{\phi}}^{(i)} \neq \underline{\Delta\phi}^{(i)}}}^{B} E\left\{e^{\lambda_0(\hat{\eta}_i - \eta_i)} \middle| \underline{\Delta\phi}_i\right\} \tag{C-1}$$

where "E" denotes the expectation operator and λ_0 is the Chernoff parameter to be optimized. The remainder of this appendix is devoted to an evaluation of $E\left\{e^{\lambda_0(\hat{\eta}_i - \eta_i)} \middle| \underline{\Delta\phi}^{(i)}\right\}$. For simplicity of notation, we shall drop the subscript "i" with the understanding that we are referring to the i*th* branch in the trellis paths under consideration.

From the definitions of η, and $\hat{\eta}$ we can write the difference $\hat{\eta} - \eta$ in the matrix form

$$\hat{\eta} - \eta = \underline{w}^{*T}\mathbf{F}\underline{w} \tag{C-2}$$

where

$$\underline{w} = \begin{bmatrix} w(\underline{\Delta\phi}) \\ w(\underline{\Delta\hat{\phi}}) \end{bmatrix}; \quad \mathbf{F} = \begin{bmatrix} 1 & 0 \\ 0 & -1 \end{bmatrix} \tag{C-3}$$

and the "T" denotes the transpose operation. Here

$$w(\underline{\Delta\phi}) = \sum_{n=0}^{N-1} r_{k-n} e^{-j\sum_{m=0}^{N-n-2}\Delta\phi_{k-n-m}}$$

$$w(\underline{\Delta\hat{\phi}}) = \sum_{n=0}^{N-1} r_{k-n} e^{-j\sum_{m=0}^{N-n-2}\Delta\hat{\phi}_{k-n-m}} \tag{C-4}$$

with

$$r_k = \sqrt{2P}e^{j(\theta+\phi_k)} + n_k \tag{C-5}$$

Substituting (C-2) into (C-1), we get an upper bound of the form given in [8: Eq. (21)] which can thus be evaluated as (see [12] for a derivation of the result)

$$E\left\{e^{\lambda_0 \underline{w}^{*T}\mathbf{F}\underline{w}} | \underline{\Delta\phi}\right\} = \frac{\exp\left\{\lambda_0 \underline{\mu}^{*T}\mathbf{F}(\mathbf{I}-2\lambda_0\mathbf{R}^*\mathbf{F})^{-1}\underline{\mu}\right\}}{\det(\mathbf{I}-2\lambda_0\mathbf{R}^*\mathbf{F})} \tag{C-6}$$

where I is the identity matrix,

$$\underline{\mu} \triangleq E\left\{\underline{w}|\underline{\Delta\phi}\right\} = \begin{bmatrix} E\left\{w(\underline{\Delta\hat{\phi}})|\underline{\Delta\phi}\right\} \\ E\left\{w(\underline{\Delta\phi})|\underline{\Delta\phi}\right\} \end{bmatrix} = \sqrt{2P}\begin{bmatrix} \sum_{n=0}^{N-1} e^{j(\theta+\phi_{k-n})} e^{-j\sum_{m=0}^{N-n-2}\Delta\hat{\phi}_{k-n-m}} \\ \sum_{n=0}^{N-1} e^{j(\theta+\phi_{k-n})} e^{-j\sum_{m=0}^{N-n-2}\Delta\phi_{k-n-m}} \end{bmatrix} \tag{C-7}$$

and

$$\mathbf{R} = \frac{1}{2}E\left\{(\underline{w}-\underline{\mu})^*(\underline{w}-\underline{\mu})^T|\underline{\Delta\phi}\right\} = \frac{1}{2}\begin{bmatrix} \frac{2N_0N}{T_s} & \frac{2N_0\delta^*}{T_s} \\ \frac{2N_0\delta}{T_s} & \frac{2N_0N}{T_s} \end{bmatrix} \tag{C-8}$$

with

$$\delta \triangleq \sum_{n=0}^{N-1} e^{j\sum_{m=0}^{N-n-2}\left(\Delta\phi_{k-n-m}-\Delta\hat{\phi}_{k-n-m}\right)} \triangleq \sum_{n=0}^{N-1} e^{j\sum_{m=0}^{N-n-2}\delta\phi_{k-n-m}} \tag{C-9}$$

To evaluate (C-6) we need to compute the determinant and inverse of $(\mathbf{I}-2\lambda_0\mathbf{R}^*\mathbf{F})$. Using (C-3) and (C-8) these are evaluated, respectively, as

$$\det(\mathbf{I}-2\lambda_0\mathbf{R}^*\mathbf{F}) = 1 - 4\lambda_0^2\frac{N_0^2N^2}{T_s^2} + 4\lambda_0^2\frac{N_0^2|\delta|^2}{T_s^2} \tag{C-10}$$

and

$$(\mathbf{I}-2\lambda_0\mathbf{R}^*\mathbf{F})^{-1} = \frac{1}{\det(\mathbf{I}-2\lambda_0\mathbf{R}^*\mathbf{F})}\begin{bmatrix} 1+2\lambda_0\frac{N_0N}{T_s} & -2\lambda_0\frac{N_0\delta}{T_s} \\ 2\lambda_0\frac{N_0\delta^*}{T_s} & 1-2\lambda_0\frac{N_0N}{T_s} \end{bmatrix} \tag{C-11}$$

Finally, using (C-10) and (C-11) in (C-6) gives

$$E\left\{e^{\lambda_0 \underline{w}^{*T}\underline{F}\underline{w}} \middle| \underline{\Delta\phi}\right\} = \frac{\exp\left\{-\frac{E_s}{N_0}\frac{\lambda(1-\lambda N)\left[N^2-|\delta|^2\right]}{1-\lambda^2\left[N^2-|\delta|^2\right]}\right\}}{1-\lambda^2\left[N^2-|\delta|^2\right]} \qquad \text{(C-12)}$$

where $E_S = PT_S$ and

$$\lambda \triangleq 2\lambda_0 \frac{N_0}{T_s} \qquad \text{(C-13)}$$

Reinserting the subscript "i" on δ to denote the fact that (C-12) applies to the *ith* trellis branch, and substituting the result in (C-1) gives the desired Chernoff bound on pairwise error probability, namely,

$$\Pr\left\{\sum_{i=1}^{B}\hat{\eta}_i > \sum_{i=1}^{B}\eta_i \middle| \underline{\Delta\phi}\right\} \le \prod_{\substack{i=1 \\ \underline{\Delta\hat{\phi}}^{(i)} \neq \underline{\Delta\phi}^{(i)}}}^{B} \frac{\exp\left\{-\frac{E_s}{N_0}\frac{\lambda(1-\lambda N)\left[N^2-|\delta_i|^2\right]}{1-\lambda^2\left[N^2-|\delta_i|^2\right]}\right\}}{1-\lambda^2\left[N^2-|\delta_i|^2\right]} \qquad \text{(C-14)}$$

The value of λ that minimizes the bound of (C-14) must be found by numerical evaluation.

Appendix D

Asymptotic Evaluation of Certain Integrals of Analytic Functions

Let f(z) and g(z) be meromorphic functions of z on the complex plane, C. Consider the integral

$$I_\Gamma(\gamma) = \int_\Gamma g(z)\exp(j\gamma f(z))dz \qquad \text{(D-1)}$$

where the contour Γ does not pass through any singularity of f(z) or g(z) and we assume that $\gamma > 0$. Although the contour is usually specified, we can clearly choose another contour Γ_0 such that the integral in (D-1) remains unchanged, i.e., $I_\Gamma(\gamma) = I_{\Gamma_0}(\gamma)$ provided that the region bounded by Γ and Γ_0 does not contain any of the singular points of the integrand. In particular, the selection of the contour Γ_0 will be an important consideration in what follows.

We now describe a procedure for evaluating (D-1) in the limit of large γ, that is, we seek the first term of an asymptotic expansion of $I_\Gamma(\gamma)$ as $\gamma \to \infty$. The following assumptions, which are applicable to the case at hand, are made:

(i) The contour of integration Γ_0 may be chosen to pass through at least one critical point z_0 of f(z), i.e., a point in C where $f'(z_0) = 0$ and the prime denotes differentiation. The critical points of f(z) on Γ_0 are assumed to be non-degenerate, i.e., $f''(z_0) \neq 0$ if $f'(z_0) = 0$.

(ii) $\mathrm{Im}\{f(z_0)\}$ is an absolute minimum of $\mathrm{Im}\{f(z)\}$ for $z \in \Gamma_0$.

(iii) The functions g(z), g(z)/f'(z), and g'(z)/f'(z) decay sufficiently rapidly as to ensure absolute convergence of the integrals that appear.

Let $\{z_i; i \in \eta\}$ denote the set of critical points of f(z) that lie along Γ_0. Let $\chi(z)$ be an infinitely differentiable function which is identically equal to unity in a small interval $\mathfrak{I}_i$ containing z_i and vanishes outside $J_i \supset \mathfrak{I}_i$ where J_i is a small neighborhood of z_i in Γ_0. Writing g(z) in the form

$$g(z) = \chi(z)g(z) + (1-\chi(z))g(z) \tag{D-2}$$

then we can easily see that $I_\Gamma(\gamma)$ can be written as a sum of integrals of the form

$$\begin{aligned} I_1(\gamma) &= \int_{K_i} g(z)\exp(j\gamma f(z))dz \\ I_2(\gamma) &= \int_{J_i} g(z)\exp(j\gamma f(z))dz \end{aligned} \tag{D-3}$$

where J_i contains a unique critical point of f(z), namely z_i, and K_i is a contour (possibly infinite) which contains no critical points of f(z). If K_i is unbounded, then the integral over K_i is understood as an improper integral in the standard manner. The contour Γ_0 is composed of the union of $\{J_i, K_i; i \in \eta\}$. Also, the function g(z) vanishes at the end points of J_i and K_i. We now investigate the asymptotic behavior of $I_1(\gamma)$ and $I_2(\gamma)$.

To evaluate $I_1(\gamma)$, we should map the contour line integral into an integral along a portion of the real line parameterized by the variable t. Thus, let $\zeta_i(t)$ be a continuously differentiable mapping, with nowhere vanishing derivative, of the interval $t \in (0,1)$ onto the contour K_i. Then, keeping in mind that K_i contains no critical points of f(z), the first integral in (D-3) can be written as

$$\begin{aligned} I_1(\gamma) &= \int_0^1 g(\zeta(t))\exp(j\gamma f(\zeta(t)))\zeta'(t)dt \\ &= \int_0^1 \frac{\frac{d}{dt}\exp(j\gamma f(\zeta(t)))}{j\gamma f'(\zeta(t))} g(\zeta(t))dt \\ &= \frac{1}{j\gamma}\int_0^1 \frac{g(\zeta(t))}{f'(\zeta(t))} d\exp(j\gamma f(\zeta(t))) \end{aligned} \tag{D-4}$$

Integrating by parts results in

$$I_1(\gamma) = \frac{g(\zeta(t))\exp(j\gamma f(\zeta(t)))}{j\gamma f'(\zeta(t))}\Bigg|_0^1 - \frac{1}{j\gamma}\int_0^1 \exp(j\gamma f(\zeta(t)))\frac{d}{dt}\left(\frac{g(\zeta(t))}{f'(\zeta(t))}\right)dt \tag{D-5}$$

The first term in (D-5) vanishes in view of the assumption of rapid decay of $g(z)/f'(z)$ if K_i is infinite, and the vanishing of $g(z)$ at the end points $t = 0,1$. Therefore,

$$I_1(\gamma) = -\frac{1}{j\gamma}\int_0^1 \exp\big(j\gamma f(\zeta(t))\big)\frac{d}{dt}\left(\frac{g(\zeta(t))}{f'(\zeta(t))}\right)dt \tag{D-6}$$

whose absolute value is upper bounded by

$$|I_1(\gamma)| \le \frac{1}{\gamma}\int_0^1 \exp\big(-\gamma \mathrm{Im}\{f(\zeta(t))\}\big)\left|\frac{d}{dt}\left(\frac{g(\zeta(t))}{f'(\zeta(t))}\right)\right|dt \tag{D-7}$$

Finally, since by assumption (ii),

$$\min_t \mathrm{Im}\{f(z)\} = \mathrm{Im}\{f(z_i)\} \triangleq c_i \tag{D-8}$$

then, in the integration interval of (D-7),

$$\exp\big(-\gamma \mathrm{Im}\{f(\zeta(t))\}\big) \le \exp(-\gamma c_i) \tag{D-9}$$

and hence,

$$|I_1(\gamma)| \le C_i\frac{1}{\gamma}\exp(-\gamma c_i); \quad C_i = \int_0^1\left|\frac{d}{dt}\left(\frac{g(\zeta(t))}{f'(\zeta(t))}\right)\right|dt \tag{D-10}$$

The second integral of (D-3) involves evaluation in the neighborhood of the critical point z_i under the assumption that the critical point z_i is a minimum of $\mathrm{Im}\{f(z)\}$, $z \in \Gamma_0$. The asymptotic expansion of this integral is given in [13: Chap. 8]. Using the first term as an approximation to $I_2(\gamma)$, we obtain

$$I_2(\gamma) \cong \sqrt{\frac{2\pi j}{\gamma f''(z_i)}}\exp\big(j\gamma f(z_i)\big)g(z_i) \tag{D-11}$$

Once again considering the absolute value of this integral, we get

$$|I_2(\gamma)| \cong D_i\frac{1}{\sqrt{\gamma}}\exp(-\gamma c_i); \quad D_i = \left|\sqrt{\frac{2\pi j}{f''(z_i)}}g(z_i)\right| \tag{D-12}$$

which clearly dominates $|I_1(\gamma)|$ of (D-10). It is easy to see that the contribution of the critical points which are not minimum of $\mathrm{Im}\{f(z)\}$ are dominated by $|I_2(\gamma)|$. Therefore, for large γ, $I_\Gamma(\gamma)$ is asymptotically given by

$$I_\Gamma(\gamma) \cong \sum_{i \varepsilon \eta} \sqrt{\frac{2\pi j}{\gamma f''(z_i)}} \exp(j\gamma f(z_i)) g(z_i) \qquad \text{(D-13)}$$

where the summation is over all the critical points z_i of f(z) that are absolute minima of Im{f(z)} on Γ_0. Note that if z_0 is the only such critical point along the contour Γ_0, then the summation in (D-13) contains only a single term. As we shall see, in special cases of the above general theory, it is possible to choose the contour Γ_0 such that this is true and hence the numerical evaluation is considerably simplified.

One very special case of the above occurs when f(z) and g(z) are of the form [see (73)]

$$g(z) = \frac{1}{z} \prod_{i=1}^{B} \frac{1}{\xi_i^2 z^2 + 1}$$

$$f(z) = \sum_{i=1}^{B} \frac{\xi_i z \beta_{2i} + j \xi_i^2 z^2 \beta_1}{\xi_i^2 z^2 + 1} \qquad \text{(D-14)}$$

where ξ_i, β_1, and β_{2i} are real coefficients (note that $\xi_1 = 1$) and the contour Γ is the straight line extending from $z = -\infty + j\varepsilon$ to $z = \infty + j\varepsilon$. It is sufficient to have $\varepsilon > 0$ to avoid the pole of g(z) at the origin. However, as mentioned above we should redefine the contour (to Γ_0) so that it passes through a critical point of f(z). For B = 1, it can be shown that there are two critical points both of which lie along the imaginary z axis, i.e., $z_i = j\rho_i$; i = 1,2. One of these critical points, say ρ_1, lies below the singularity of g(z) at $z = j\xi_1 = j$ whereas the second critical point, say ρ_2, lies above this singularity. Thus, in accordance with the above, if we choose $\varepsilon = \rho_1$ then the contour Γ_0 will pass through only one critical point of f(z) and not cross any of the singularities. Hence, the summation in (D-13) reduces to just a single term. The details of the evaluation are carried out in Section 8.2 of the main body of the report.

When B > 1, then

$$f'(z) = -\sum_{i=1}^{B} \xi_i \frac{\beta_{2i} \xi_i^2 z^2 - 2j\beta_1 \xi_i z - \beta_{2i}}{\left(\xi_i^2 z^2 + 1\right)^2} = 0 \qquad \text{(D-15)}$$

which, in general, yields 2 + 4(D-1) critical points of f(z). Since it is not, in

general, true that all the critical points lie on the imaginary z axis, one must evaluate these critical points numerically for each particular case and then select the contour Γ_0 appropriately as discussed above. It can be shown however (see Appendix E), that for arbitrary B, there exists a unique critical point, say z_0, on the imaginary z axis in the interval $0 \le z \le j$. Therefore, since $\xi_i \le 1$ for $1 \le i \le B$ (see the definition of ξ_i in Eq. (72) of the main text), and thus, aside from the singularity of g(z) at z = 0, all of the singularities of g(z) and f(z) occur along the imaginary z axis in the interval $j \le z \le j\infty$, it is sufficient to find this unique critical point $z_0 = jy_0$ $(0 \le y_0 \le 1)$ and choose the contour Γ_0 to pass through it.

It remains to satisfy condition (ii). Let v(z) = Im{f(z)}. Then, from the computations in Appendix E, it is clear that

$$\frac{\partial^2 v(x+jy)}{\partial y^2} < 0 \qquad \text{(D-16)}$$

for $0 \le y \le 1$. Since v(z) is harmonic, i.e., for all analytic functions f(z), we have

$$\frac{\partial^2 v(x+jy)}{\partial y^2} + \frac{\partial^2 v(x+jy)}{\partial x^2} = 0 \qquad \text{(D-17)}$$

then

$$\frac{\partial^2 v(x+jy)}{\partial x^2} > 0 \qquad \text{(D-18)}$$

and thus the critical point $z_0 = jy_0$ is a *local* minimum of v(z) along the line $z = x + jy_0$ parallel to the x axis. It is straightforward to show that the contour Γ_0 can be deformed to a contour Γ_0' such that

$$I_{\Gamma_0}(\gamma) = I_{\Gamma_0'}(\gamma) \qquad \text{(D-19)}$$

and where $z_0 = jy_0$ is the *global* minumum of v(z) on Γ_0'. Thus, condition (ii) is satisfied for the critical point z_0.

Appendix E

Proof That There Exists a Unique Critical Point of f(z) Along the Imaginary z Axis in the Interval 0 < z < j

Here we present a proof that the function f(z) (defined in Eq. (73) of the main text or Eq. (D-14) of Appendix D) has a unique critical point (i.e., the value of z where f'(z) = 0) along the imaginary z axis in the interval 0 < z < j. Consider writing the derivative f'(z) along the imaginary z axis in the form

$$f'(jy) = \sum_{i=1}^{B} f_i'(jy) \tag{E-1}$$

where, from (D-15),

$$f_i'(jy) = \xi_i \frac{\beta_{2i}\xi_i^2 y^2 - 2\beta_1 \xi_i y + \beta_{2i}}{\left(1 - \xi_i^2 y^2\right)^2} \tag{E-2}$$

Evaluating (E-2) at y = 0, we have

$$f_i'(0) = \beta_{2i}\xi_i = \frac{N^2 - |\delta_i|^2}{\left(N^2 - |\delta_{i_{\min}}|^2\right)^{1/2}} > 0 \tag{E-3}$$

At y = 1, (E-2) becomes

$$\begin{aligned} f_i'(j) &= \xi_i \frac{\beta_{2i}\xi_i^2 - 2\beta_1\xi_i + \beta_{2i}}{\left(1 - \xi_i^2\right)^2} \\ &= \left(1 - \frac{N^2 - |\delta_i|^2}{N^2 - |\delta_{i_{\min}}|^2}\right)^{-2} \left[\frac{\left(N^2 - |\delta_i|^2\right)^{3/2}}{N^2 - |\delta_{i_{\min}}|^2} - \frac{2N\left(N^2 - |\delta_i|^2\right)^{1/2}}{\left(N^2 - |\delta_{i_{\min}}|^2\right)^{1/2}} + \left(N^2 - |\delta_i|^2\right)^{1/2}\right] \end{aligned} \tag{E-4}$$

The first factor in (E-4) is clearly positive. We now wish to show that the second (bracketed) factor in (E-4) is negative. The steps are as follows:

$$\frac{\left(N^2-|\delta_i|^2\right)^{3/2}}{N^2-|\delta_{i_{\min}}|^2}-\frac{2N\left(N^2-|\delta_i|^2\right)^{1/2}}{\left(N^2-|\delta_{i_{\min}}|^2\right)^{1/2}}+\left(N^2-|\delta_i|^2\right)^{1/2}$$

$$=\frac{\left(N^2-|\delta_i|^2\right)^{1/2}}{N^2-|\delta_{i_{\min}}|^2}\left[N^2-|\delta_i|^2-2N\left(N^2-|\delta_{i_{\min}}|^2\right)^{1/2}+N^2-|\delta_{i_{\min}}|^2\right]$$

$$<\frac{\left(N^2-|\delta_i|^2\right)^{1/2}}{N^2-|\delta_{i_{\min}}|^2}\left[N^2-|\delta_i|^2-2\left(N^2-|\delta_{i_{\min}}|^2\right)+N^2-|\delta_{i_{\min}}|^2\right]$$

$$=\frac{\left(N^2-|\delta_i|^2\right)^{1/2}}{N^2-|\delta_{i_{\min}}|^2}\left[|\delta_{i_{\min}}|^2-|\delta_i|^2\right]\le 0$$

(E-5)

Thus, since each term in f'(jy) changes sign in the interval $0 \le y \le 1$, there must be at least one value of y at which f'(jy) = 0, i.e., at least one critical point of f(z) occurs in the interval $0 < z < j$. It now remains to show that there is only one such point, i.e., the critical point of f(z) that occurs in the interval $0 < z < j$ is unique. We shall do this by showing that f''(z) is always negative in the interval $0 \le z \le j$ and thus f'(z) is monotonically decreasing in this same interval.

Consider the derivative of (E-2). After considerable simplification and use of the definitions of β_1, β_{2i}, and ξ_i in (72), we obtain

$$f_i'(jy)=\frac{-2\left(N^2-|\delta_i|^2\right)^{1/2}v^5+6Nv^4-4\left(N^2-|\delta_i|^2\right)^{1/2}v^3-4Nv^2+6\left(N^2-|\delta_i|^2\right)^{1/2}v-2N}{\left(1-v^2\right)^4};$$

$$v=\frac{\left(N^2-|\delta_i|^2\right)^{1/2}}{\left(N^2-|\delta_{i_{\min}}|^2\right)^{1/2}}y=\xi_i y$$

(E-6)

It is straightforward to show that the sum of the first, third, and fifth terms of the numerator are non-negative in the interval $0 \le v \le 1$ (or equivalently $0 \le y \le (\xi_i)^{-1}$). In particular,

$$-2\left(N^2-|\delta_i|^2\right)^{1/2}v^5-4\left(N^2-|\delta_i|^2\right)^{1/2}v^3+6\left(N^2-|\delta_i|^2\right)^{1/2}v$$
$$=-2\left(N^2-|\delta_i|^2\right)^{1/2}v(v^4+2v^2-3)\geq 0 \quad \text{for } 0\leq v\leq 1 \tag{E-7}$$

Thus,

$$-2\left(N^2-|\delta_i|^2\right)^{1/2}v^5-4\left(N^2-|\delta_i|^2\right)^{1/2}v^3+6\left(N^2-|\delta_i|^2\right)^{1/2}v$$
$$\leq -2Nv^5-4Nv^3+6Nv \quad \text{for } 0\leq v\leq 1 \tag{E-8}$$

Substituting (E-8) in (E-6), we get

$$f_i''(jy)\leq \frac{-2Nv^5+6Nv^4-4Nv^3-4Nv^2+6Nv-2N}{\left(1-v^2\right)^4}$$
$$=\frac{-2N\left(v^5-3v^4+2v^3+2v^2-3v+1\right)}{\left(1-v^2\right)^4}$$
$$=\frac{-2N(1-v)^3}{\left(1-v^2\right)^3}\leq 0; \quad 0\leq v\leq 1 \tag{E-9}$$

Finally, since the derivative of (E-1) is the sum of the derivatives of each term in the summation, and recalling from (72) that $\xi_i \leq 1$, then from (E-9) we obtain the desired result, namely,

$$f_i''(jy)\leq 0; \quad 0\leq y\leq 1 \tag{E-10}$$

or, equivalently, $f_i'(jy)$ is monotonically decreasing in $0 \leq y \leq 1$. Q.E.D.

Although not of specific interest, it can also be shown that the critical points of f(z) that do not lie on the imaginary z axis occur in pairs that are symmetric about this axis. That is, if $z_0 = x_0 + jy_0$ is a critical point, i.e., $f'(z_0) = 0$, then $z_1 = -x_0+jy_0$ satisfies $f'(z_1) = 0$.

TECHNICAL REPORT STANDARD TITLE PAGE

1. Report No. JPL Publication 89-38	2. Government Accession No.	3. Recipient's Catalog No.
4. Title and Subtitle Multiple Symbol Differential Detection of Uncoded and Trellis Coded MPSK		5. Report Date November 15, 1989 6. Performing Organization Code
7. Author(s) Dariush Divsalar, Marvin K. Simon, and Mehrdad Shahshahani		8. Performing Organization Report No.
9. Performing Organization Name and Address JET PROPULSION LABORATORY California Institute of Technology 4800 Oak Grove Drive Pasadena, California 91109		10. Work Unit No. 11. Contract or Grant No. NAS7-918 13. Type of Report and Period Covered JPL Publication
12. Sponsoring Agency Name and Address NATIONAL AERONAUTICS AND SPACE ADMINISTRATION Washington, D.C. 20546		14. Sponsoring Agency Code RE4 BP-643-10-05-01-00

15. Supplementary Notes

16. Abstract

A differential detection technique for MPSK, which uses a multiple symbol observation interval, is presented and its performance analyzed and simulated. The technique makes use of maximum-likelihood sequence estimation of the transmitted phases rather than symbol-by-symbol detection as in conventional differential detection. As such the performance of this multiple symbol detection scheme fills the gap between conventional (two-symbol observation) differentially coherent detection of MPSK and ideal coherent of MPSK with differential encoding. The amount of improvement gained over conventional differential detection depends on the number of phases, M, and the number of additional symbol intervals added to the observation. What is particularly interesting is that substantial performance improvement can be obtained for only one or two additional symbol intervals of observation. The analysis and simulation results presented are for uncoded and trellis coded MPSK.

17. Key Words (Selected by Author(s))	18. Distribution Statement
Communications Statistics and Probability	Unclassified - Unlimited

19. Security Classif. (of this report)	20. Security Classif. (of this page)	21. No. of Pages	22. Price
Unclassified	Unclassified	74	